

General model and toolkit for the ionization of three or more electrons in strongly driven molecules using an effective Coulomb potential for the interaction between bound electrons

G. P. Katsoulis , M. B. Peters , and A. Emmanouilidou*Department of Physics and Astronomy, University College London, Gower Street, London WC1E 6BT, United Kingdom*

(Received 30 November 2023; accepted 21 February 2024; published 12 March 2024)

We formulate a general three-dimensional semiclassical model for the study of correlated multielectron escape during fragmentation of molecules driven by intense infrared laser pulses. We do so in the context of triple ionization of strongly driven HeH_2^+ . Our model fully accounts for the singularity in the Coulomb potentials of a recolliding electron with the core and a bound electron with the core as well as for the interaction of a recolliding electron with a bound electron. This model also accounts for the magnetic field of the laser pulse. To avoid artificial autoionization, our model employs effective potentials to treat the interaction between bound electrons. We focus on triple and double ionization as well as frustrated triple and frustrated double ionization. In these processes, we identify and explain the main features of the sum of the kinetic energies of the final ion fragments. We find that frustrated double ionization is a major ionization process, and we identify the different channels and hence different final fragments that are obtained through frustrated double ionization. Also, we discuss the differences between frustrated double and triple ionization.

DOI: [10.1103/PhysRevA.109.033106](https://doi.org/10.1103/PhysRevA.109.033106)

I. INTRODUCTION

Multielectron ionization and the formation of highly excited Rydberg states are fundamental processes in molecules driven by intense and infrared laser pulses. Rydberg states have a wide range of applications, such as acceleration of neutral particles [1], spectral features of photoelectrons [2], and formation of molecules via long-range interactions [3]. Electron-nuclear correlated multiphoton resonance excitation was shown to be the mechanism responsible for the formation of Rydberg states in weakly driven H_2 [4]. This process was shown to merge with frustrated double ionization for H_2 (strongly) driven by intense infrared laser fields [5,6]. In frustrated ionization an electron first tunnel ionizes in the driving laser field. Then, due to the electric field, this electron is recaptured by the parent ion in a Rydberg state [7].

Most studies on strongly driven molecules address double and frustrated double ionization of two-electron molecules [5,6,8–18]. However, there are scarcely any theoretical studies on three-electron ionization and formation of Rydberg states during the fragmentation of strongly driven molecules. The reason is that accounting for both multielectron and nuclear motion is a formidable task. This is corroborated by the few theoretical studies on three-electron ionization of strongly driven atoms, a simpler but still highly challenging task. Mostly formulated in the dipole approximation, these studies on atoms employ lower-dimensionality classical [19,20] and

quantum-mechanical [21,22] models to reduce the complexity and computational resources required. However, lower dimensionality results in an inaccurate description of electron-electron interaction during triple ionization. Currently, only classical or semiclassical three-dimensional (3D) models of triple ionization of atoms are available [20,23–26].

In Refs. [27,28] we argued that the main disadvantage of available classical and quantum models of triple ionization in atoms is their softening of the Coulomb interaction of each electron with the core. In quantum-mechanical models, this interaction is softened to obtain a computationally tractable problem. However, in classical and semiclassical models, softening the Coulomb singularity is fundamental and relates to unphysical autoionization. Classically there is no lower energy bound. Hence, when a bound electron undergoes a close encounter with the core, the Coulomb singularity allows this electron to acquire a very negative energy. Through the Coulomb interaction, this energy can be shared by another bound electron, potentially leading to its artificial escape.

To avoid artificial autoionization, most classical and semiclassical models of triple ionization of strongly driven atoms soften the Coulomb potential [20,23,24] or add Heisenberg potentials [29] (effective softening) to mimic the Heisenberg uncertainty principle and prevent each electron from having a close encounter with the core [25,26]. However, softening the Coulomb potential does not allow for an accurate description of electron scattering from the core [30,31]. This is due to the exponential decrease of the ratio of the scattering amplitude for the soft-core potential over the one for the Coulomb potential with increasing momentum transfer [30,31]. For recollisions [32], this implies that soft potentials are quite inaccurate for high-energy recolliding electrons that backscatter. Indeed, we have shown [27,28] that the ionization spectra obtained with the Heisenberg model

Published by the American Physical Society under the terms of the [Creative Commons Attribution 4.0 International license](https://creativecommons.org/licenses/by/4.0/). Further distribution of this work must maintain attribution to the author(s) and the published article's title, journal citation, and DOI.

differ from experimental ones obtained for driven Ne and Ar [33–39].

Here we formulate a general 3D semiclassical model of multielectron ionization and fragmentation of strongly driven molecules while fully accounting for the magnetic field of the laser pulse. The main premise in our model is that two interactions are most important during a recollision or return of an electron to the core and hence are treated exactly. We account for the singularity in the Coulomb potential between each electron, bound or quasifree, and the core. Quasifree refers to a recolliding electron or an electron escaping to the continuum. Also, we treat exactly the Coulomb potential between each pair of a quasifree and a bound electron and hence the transfer of energy from a quasifree to a bound electron. However, accounting for the singularity in the electron-core interaction implies we need to avoid unphysical autoionization that can take place through energy transfer between bound electrons. We do so by approximating the energy transfer from a bound to a bound electron via the use of effective Coulomb potentials. We refer to this model that accurately accounts for all Coulomb interactions and only employs approximate effective Coulomb potentials to describe the bound-bound electron interaction as the ECBB model. This is a sophisticated model that identifies during time propagation whether an electron is quasifree or bound, that is, in the ECBB model, we decide on the fly if the full or effective Coulomb potential describes the interaction between a pair of electrons. We do so by using a set of simple criteria detailed below.

The ECBB model for strongly driven molecules is a generalization of the ECBB model we have previously developed for strongly driven atoms [27,28]. For atoms, we have shown that the ECBB model results in triple ionization spectra of strongly driven Ne that are in excellent agreement with experiment [28]. The main difficulty in generalizing the ECBB model to molecules is the formulation of the effective Coulomb potential between a pair of bound electrons in the presence of many nuclei. In atoms, the effective Coulomb potential is obtained by assuming that a bound electron has a charge distribution centered around the atomic core. In molecules, we assume that an electron creates an effective potential that is the sum of the effective Coulomb potentials with respect to each nucleus separately, i.e., each effective Coulomb potential is the same as for an atom. However, each atomic effective Coulomb potential is weighted by an approximate expression for the probability to find the electron that creates this potential at a given position around this nucleus.

Using the ECBB model, we address triple and double ionization in the triatomic molecule HeH_2^+ when driven by a linearly polarized laser pulse. We also address the formation of Rydberg states via frustrated ionization. Employing the HeH_2^+ molecule allows us to directly compare the results for triple, double, and frustrated triple ionization obtained with the ECBB model in this study and with a predecessor of the ECBB model obtained in previous work [40]. This previous model determined on the fly whether an electron is quasifree or bound, as the ECBB model does, but this was done using a set of criteria less sophisticated than the ones employed in the ECBB model for atoms [27,28] and molecules in the present work. Also, in this previously employed model the interaction

of a pair of bound electrons was set equal to zero. As a result, in Ref. [40] we could only address frustrated triple ionization where two electrons ionize and one electron remains bound in a Rydberg state. Here, since we account, via effective potentials, for the interaction between bound electrons, we can also address frustrated double ionization. In this process, one electron ionizes, the other remains bound in the ground state of one of the He or H fragments, and another electron remains bound in a Rydberg state of one of the fragments.

Here we address both triple and double ionization as well as frustrated triple and double ionization and obtain the sum of the kinetic energies of the atomic fragments, referred to as kinetic energy release. We find that the atomic fragments are moving faster when fragmentation of HeH_2^+ is described with the ECBB model compared to its predecessor [27,28]. This is consistent with our finding that the electron-electron escape to the continuum is more correlated when the process is described with the ECBB model, since it allows for energy transfer between bound electrons. Higher correlation results in faster electron escape, leading to Coulomb explosion of the nuclei at smaller distances, eventually resulting in higher kinetic energies. While in frustrated triple ionization (FTI) two electrons ionize and one remains bound in a Rydberg state, in frustrated double ionization (FDI) one electron ionizes, one electron remains bound in the ground state with a quantum number $n = 1$, and another electron remains bound in a Rydberg state. We find that, in three-electron molecules, FTI and FDI proceed via two pathways, first identified in FDI of the strongly driven two-electron molecule H_2 [6]. One electron ionizes early on (first step), while the remaining bound electron does so later in time (second step). If the second (first) ionization step is frustrated, we label the FTI and FDI pathways as A and B, respectively.

II. METHOD

In what follows, we describe in detail the formulation of the ECBB model for strongly driven molecules. The ECBB model resolves unphysical autoionization in 3D semiclassical models that fully account for the Coulomb singularity. Also, we formulate the ECBB model in the nondipole approximation fully accounting for the magnetic-field component of the laser field. Finally, both electrons and the cores are propagated in time.

A. Definition of the effective charge and potential

In what follows, the cores are assigned indices in the interval $[1, N_c]$, where N_c is the number of cores. The remaining indices in the interval $[N_c + 1, N]$, with N the number of particles, are assigned to the electrons. For each electron j , we define an effective charge $\zeta_{j,n}(t)$ associated with each core n as [41]

$$\zeta_{j,n}(t) = \begin{cases} Q_n, & \mathcal{E}_j(t) \leq \mathcal{E}_{1s}^n \\ (Q_n/\mathcal{E}_{1s}^n)\mathcal{E}_j(t), & \mathcal{E}_{1s}^n < \mathcal{E}_j(t) < 0 \\ 0, & \mathcal{E}_j(t) \geq 0, \end{cases} \quad (1)$$

where Q_n is the charge of the core n , \mathcal{E}_{1s}^n is the ground-state energy of a hydrogenic atom with core charge Q_n , i.e., $\mathcal{E}_{1s}^n =$

$-\mathcal{Q}_n^2/2$, and $\mathcal{E}_j(t)$ is the energy of electron j given by

$$\begin{aligned} \mathcal{E}_j(t) = & \frac{[\tilde{\mathbf{p}}_j - \mathcal{Q}_j \mathbf{A}(\mathbf{r}_j, t)]^2}{2m_j} + \sum_{n=1}^{N_c} \frac{\mathcal{Q}_n \mathcal{Q}_j}{|\mathbf{r}_n - \mathbf{r}_j|} - \mathcal{Q}_j \mathbf{r}_j \cdot \mathbf{E}(\mathbf{r}_j, t) \\ & + \sum_{n=1}^{N_c} \sum_{\substack{i=N_c+1 \\ i \neq j}}^N c_{i,j}(t) C_{i,n}(\mathcal{E}_i, |\mathbf{r}_1 - \mathbf{r}_i|, \dots, |\mathbf{r}_{N_c} - \mathbf{r}_i|) \\ & \times V_{\text{eff}}(\zeta_{i,n}(t), |\mathbf{r}_n - \mathbf{r}_j|), \end{aligned} \quad (2)$$

where $\mathbf{A}(\mathbf{r}_j, t)$ is the vector potential and $\mathbf{E}(\mathbf{r}_j, t) = -\frac{\partial \mathbf{A}(\mathbf{r}_j, t)}{\partial t}$ is the electric field. The effective potential that an electron j experiences at a distance $|\mathbf{r}_n - \mathbf{r}_j|$ from the core n due to the charge of electron i is given by [41]

$$\begin{aligned} V_{\text{eff}}(\zeta_{i,n}(t), |\mathbf{r}_n - \mathbf{r}_j|) \\ = \frac{1 - (1 + \zeta_{i,n} |\mathbf{r}_n - \mathbf{r}_j|) e^{-2\zeta_{i,n} |\mathbf{r}_n - \mathbf{r}_j|}}{|\mathbf{r}_n - \mathbf{r}_j|}. \end{aligned} \quad (3)$$

Here $V_{\text{eff}}(\zeta_{i,n}(t), |\mathbf{r}_n - \mathbf{r}_j|)$ is a repulsive potential with limiting value of $\zeta_{i,n}$ when $|\mathbf{r}_n - \mathbf{r}_j| \rightarrow 0$. To avoid artificial autoionization, we have to ensure that the charge $\zeta_{i,n}$ has a fixed value in this limit. One way to do so is by setting $\zeta_{i,n}$ equal to the nuclear charge \mathcal{Q}_n for electron energies $\mathcal{E}_j(t)$ less than the hydrogenic ground-state energy \mathcal{E}_{1s}^n [see Eq. (1)]. For electron energies greater than \mathcal{E}_{1s}^n , electron j is less bound, which is accounted for by taking $\zeta_{i,n}$ to be only a fraction of the charge \mathcal{Q}_n in Eq. (1).

To generalize this effective Coulomb potential to molecules, in Eq. (2) we assume that an electron i screens each core n separately as if it were an atom, with probability $|C_{i,n}|^2$ given by

$$C_{i,n}(\mathcal{E}_i, |\mathbf{r}_1 - \mathbf{r}_i|, \dots, |\mathbf{r}_{N_c} - \mathbf{r}_i|) = \frac{\rho_{i,n}}{\sum_{n'=1}^{N_c} \rho_{i,n'}}, \quad (4)$$

with

$$\rho_{i,n}(t) = |\psi(\zeta_i, |\mathbf{r}_n - \mathbf{r}_i|)|^2 = \frac{\zeta_{i,n}^3}{\pi} e^{-2\zeta_{i,n}(t)|\mathbf{r}_n - \mathbf{r}_i|}. \quad (5)$$

Hence, we approximate the wave function of each bound electron i with a $1s$ hydrogenic wave function around each core. In addition, we are distributing the charge of a bound electron i among the different cores according to the probability density of electron i with respect to each core. Hence, the total potential that a bound electron j experiences due to a bound electron i is given by

$$\sum_{n=1}^{N_c} C_{i,n}(\mathcal{E}_i, |\mathbf{r}_1 - \mathbf{r}_i|, \dots, |\mathbf{r}_{N_c} - \mathbf{r}_i|) V_{\text{eff}}(\zeta_{i,n}(t), |\mathbf{r}_n - \mathbf{r}_j|), \quad (6)$$

where $C_{i,n}(\mathcal{E}_i, |\mathbf{r}_1 - \mathbf{r}_i|, \dots, |\mathbf{r}_{N_c} - \mathbf{r}_i|)$ is a function of the energy of electron i and the distance between electron i and the cores; $C_{i,n}(\mathcal{E}_i, |\mathbf{r}_1 - \mathbf{r}_i|, \dots, |\mathbf{r}_{N_c} - \mathbf{r}_i|)$ can be more explicitly written as $C_{i,n}(\zeta_{i,1}, \dots, \zeta_{i,N_c}, |\mathbf{r}_1 - \mathbf{r}_i|, \dots, |\mathbf{r}_{N_c} - \mathbf{r}_i|)$, but since $\zeta_{i,n} \propto \mathcal{E}_i$ we simplify the expression by only including \mathcal{E}_i .

The functions $c_{i,j}(t)$ determine whether the full Coulomb interaction or the effective $V_{\text{eff}}(\zeta_{i,n}(t), |\mathbf{r}_n - \mathbf{r}_j|)$ and

$V_{\text{eff}}(\zeta_{j,n}(t), |\mathbf{r}_n - \mathbf{r}_i|)$ potential interactions are on or off for any pair of electrons i and j during the time propagation. Specifically, the limiting values of $c_{i,j}(t)$ are zero and one. The value zero corresponds to the full Coulomb potential being turned on while the effective Coulomb potentials are off. This occurs for a pair of electrons i and j where either electron i or j is quasifree. The value one corresponds to the effective Coulomb potentials $V_{\text{eff}}(\zeta_{i,n}(t), |\mathbf{r}_n - \mathbf{r}_j|)$ and $V_{\text{eff}}(\zeta_{j,n}(t), |\mathbf{r}_n - \mathbf{r}_i|)$ being turned on while the full Coulomb potential is off. This occurs when both electrons i and j are bound. For simplicity, we choose $c_{i,j}(t)$ to change linearly with time between the limiting values zero and one [27,28]. Hence, $c_{i,j}(t)$ is defined as

$$c_{i,j}(t) = \begin{cases} 0, & c(t) \leq 0 \\ c(t), & 0 < c(t) < 1 \\ 1, & c(t) \geq 1, \end{cases} \quad (7)$$

where $c(t) = \beta(t - t_s^{i,j}) + c_0$ and c_0 is the value of $c_{i,j}(t)$ just before a switch at time $t_s^{i,j}$. We note that $c_0 \in [0, 1]$, with zero corresponding to the effective potentials being switched off and one to being switched on. Equation (7) shows that we switch on and off the effective potentials according to $c(t)$. When $c(t)$ reaches zero this means that the Coulomb potential is fully switched on and hence there should be no further change to $c_{i,j}(t)$. This is the reason $c_{i,j}(t)$ is equal to zero for $c(t) \leq 0$. Similarly, when $c(t)$ reaches one the full effective potential is on and hence there should be no further change to $c_{i,j}(t)$, which is set equal to one. A switch at time $t_s^{i,j}$ occurs if the interaction between electrons i and j changes from full Coulomb to effective Coulomb potential or vice versa. Every time during propagation that such a switch takes place, we check whether for each pair of electrons the full Coulomb force should be switched on and hence the effective potential switched off or the full Coulomb force should be switched off and the effective potential switched on. The former occurs if at time $t_s^{i,j}$ one of the two electrons in a pair of bound electrons changes to being quasifree, while the latter occurs if in a pair of a quasifree electron and a bound electron the quasifree electron becomes bound. At the start of the propagation at time t_0 , $t_s^{i,j}$ is equal to t_0 and c_0 is one for pairs of electrons that are bound and zero otherwise. To allow the effective Coulomb potential to be switched on or off in a smooth way, we choose β equal to ± 0.1 ; plus corresponds to a switch on and minus to a switch off of the effective Coulomb potential. The dipole term $-\mathcal{Q}_j \mathbf{r}_j \cdot \mathbf{E}(\mathbf{r}_j, t)$ in Eq. (2) involving the electric field does not appear in the Hamiltonian given in Eq. (8). There is no contradiction. Indeed, the gauge-invariant energy of a particle does not always coincide with the gauge-dependent Hamiltonian, as discussed in Refs. [42,43].

B. Hamiltonian of the system

The Hamiltonian of the N -body molecular system, comprised of N_c cores and $N - N_c$ electrons in the nondipole

approximation, is given by

$$\begin{aligned}
H = & \sum_{i=1}^N \frac{[\tilde{\mathbf{p}}_i - Q_i \mathbf{A}(\mathbf{r}_i, t)]^2}{2m_i} + \sum_{n=1}^{N_c} \sum_{j=n+1}^N \frac{Q_n Q_j}{|\mathbf{r}_n - \mathbf{r}_j|} \\
& + \sum_{i=N_c+1}^{N-1} \sum_{j=i+1}^N [1 - c_{i,j}(t)] \frac{Q_i Q_j}{|\mathbf{r}_i - \mathbf{r}_j|} \\
& + \sum_{i=N_c+1}^{N-1} \sum_{j=i+1}^N c_{i,j}(t) V_{i,j}, \quad (8)
\end{aligned}$$

where Q_i is the charge, m_i is the mass, \mathbf{r}_i is the position vector, and $\tilde{\mathbf{p}}_i$ is the canonical momentum vector of particle i . The mechanical momentum \mathbf{p}_i is given by

$$\mathbf{p}_i = \tilde{\mathbf{p}}_i - Q_i \mathbf{A}(\mathbf{r}_i, t). \quad (9)$$

The potential $V_{i,j}$ is given as a sum of effective potentials as

$$\begin{aligned}
V_{i,j} = & \sum_{n=1}^{N_c} [C_{j,n}(\mathcal{E}_j, |\mathbf{r}_1 - \mathbf{r}_j|, \dots, |\mathbf{r}_{N_c} - \mathbf{r}_j|) V_{\text{eff}}(\zeta_{j,n}(t), \\
& \times |\mathbf{r}_n - \mathbf{r}_i|) + C_{i,n}(\mathcal{E}_i, |\mathbf{r}_1 - \mathbf{r}_i|, \dots, |\mathbf{r}_{N_c} - \mathbf{r}_i|) \\
& \times V_{\text{eff}}(\zeta_{i,n}(t), |\mathbf{r}_n - \mathbf{r}_j|)]. \quad (10)
\end{aligned}$$

We note that the Hamiltonian we consider in Eq. (8) fully accounts for the magnetic field of the laser field via the space dependence \mathbf{r}_i of the vector potential $\mathbf{A}(\mathbf{r}_i, t)$. Investigating the effect of the magnetic field of the laser pulse in triple ionization of HeH_2^+ is beyond the focus of the present work. Such an investigation has been carried out for triple ionization of Ne [44] and can be the focus of a future work addressing triple ionization of molecules.

C. Global regularization

We perform a global regularization [45] to avoid any numerical issues arising from the Coulomb singularities. We previously used this regularization scheme, for strongly driven H_2 , to study double and frustrated double ionization within the dipole approximation [46] as well as nondipole effects in nonsequential double ionization [47]. Also, we have used this regularization to study triple ionization in the nondipole approximation in strongly driven Ar [27] and Ne [28]. In this scheme, our new coordinates involve the relative position between two particles i and j ,

$$\mathbf{q}_{ij} = \mathbf{r}_i - \mathbf{r}_j, \quad (11)$$

and their conjugate momenta

$$\rho_{ij} = \frac{1}{N} \left(\tilde{\mathbf{p}}_i - \tilde{\mathbf{p}}_j - \frac{m_i - m_j}{M} \langle \rho \rangle \right), \quad (12)$$

where

$$\langle \rho \rangle = \sum_{i=1}^N \tilde{\mathbf{p}}_i, \quad M = \sum_{i=1}^N m_i. \quad (13)$$

The inverse transformation is given by

$$\mathbf{r}_i = \frac{1}{M} \sum_{j=i+1}^N m_j \mathbf{q}_{ij} - \frac{1}{M} \sum_{j=1}^{i-1} m_j \mathbf{q}_{ji} + \langle \mathbf{q} \rangle \quad (14)$$

and

$$\tilde{\mathbf{p}}_i = \sum_{j=i+1}^N \rho_{ij} - \sum_{j=1}^{i-1} \rho_{ji} + \frac{m_i}{M} \langle \rho \rangle, \quad (15)$$

where

$$\langle \mathbf{q} \rangle = \frac{1}{M} \sum_{i=1}^N m_i \mathbf{r}_i. \quad (16)$$

Next we define a fictitious particle k for each pair of particles i and j as

$$k(i, j) = (i-1)N - \frac{i(i+1)}{2} + j, \quad (17)$$

with $j > i$ and the total number of fictitious particles being equal to $K = N(N-1)/2$. In addition, we define the parameters α_{ik} and β_{ik} as $\alpha_{ik} = 1$ and $\beta_{ik} = m_j/M$ and as $\alpha_{jk} = -1$ and $\beta_{jk} = -m_i/M$ when $k = k(i, j)$; otherwise $\alpha_{ik} = \beta_{ik} = 0$. Given the above, Eqs. (14) and (15) take the simplified forms

$$\mathbf{r}_i = \sum_{k=1}^K \beta_{ik} \mathbf{q}_k + \langle \mathbf{q} \rangle \quad (18)$$

and

$$\tilde{\mathbf{p}}_i = \sum_{k=1}^K \alpha_{ik} \rho_k + \frac{m_i}{M} \langle \rho \rangle. \quad (19)$$

D. Derivation of the time derivative of the effective charges

The Hamiltonian in Eq. (8) depends not only on positions, momenta, and time but also on the effective charges. Moreover, the Hamiltonian depends on time through the vector potential as well as through the effective charges that are time dependent. Since the effective charge of electron j is proportional to the energy $\mathcal{E}_j(t)$ [see Eq. (2)], it follows that we must obtain the derivative with respect to time of $\mathcal{E}_j(t)$. This is necessary at any time during propagation if at least two electrons are bound. Following the same procedure as in Ref. [27], we calculate the time derivative of the energy of electron j . To do so, we apply the chain rule in Eq. (2) and obtain

$$\begin{aligned}
\dot{\mathcal{E}}_j(t) = & \frac{\partial \mathcal{E}_j(t)}{\partial \mathbf{r}_j} \cdot \dot{\mathbf{r}}_j + \frac{\partial \mathcal{E}_j(t)}{\partial \tilde{\mathbf{p}}_j} \cdot \dot{\tilde{\mathbf{p}}}_j + \sum_{n=1}^{N_c} \frac{\partial \mathcal{E}_j(t)}{\partial \mathbf{r}_n} \cdot \dot{\mathbf{r}}_n + \sum_{\substack{i=N_c+1 \\ i \neq j}}^N \frac{\partial \mathcal{E}_j(t)}{\partial \mathbf{r}_i} \cdot \dot{\mathbf{r}}_i + \sum_{\substack{i=N_c+1 \\ i \neq j}}^N \frac{\partial \mathcal{E}_j(t)}{\partial \mathcal{E}_i} \dot{\mathcal{E}}_i + \frac{\partial \mathcal{E}_j(t)}{\partial t} \\
= & \frac{\partial [\mathcal{E}_j(t) - H]}{\partial \mathbf{r}_j} \cdot \dot{\mathbf{r}}_j + \sum_{n=1}^{N_c} \frac{\partial \mathcal{E}_j(t)}{\partial \mathbf{r}_n} \cdot \dot{\mathbf{r}}_n + \sum_{\substack{i=N_c+1 \\ i \neq j}}^N \frac{\partial \mathcal{E}_j(t)}{\partial \mathbf{r}_i} \cdot \dot{\mathbf{r}}_i + \sum_{\substack{i=N_c+1 \\ i \neq j}}^N \frac{\partial \mathcal{E}_j(t)}{\partial \mathcal{E}_i} \dot{\mathcal{E}}_i + \frac{\partial \mathcal{E}_j(t)}{\partial t}, \quad (20)
\end{aligned}$$

where we use $\dot{\mathbf{r}}_j = \frac{\partial \mathcal{E}_j(t)}{\partial \mathbf{p}_j}$ and $\dot{\mathbf{p}}_j = -\frac{\partial H}{\partial \mathbf{r}_j}$. In Appendix A we derive each of the terms in the chain rule in Eq. (20). Furthermore, we group together all the terms in Eq. (20) that do not depend on $\dot{\mathcal{E}}_i$ as

$$\dot{\mathcal{E}}_j(t) = f_j + \sum_{\substack{i=N_c+1 \\ i \neq j}}^N g_{j,i} \dot{\mathcal{E}}_i, \quad (21)$$

where

$$g_{j,i} = \sum_{n=1}^{N_c} c_{i,j}(t) \left[C_{i,n}(\mathcal{E}_i, |\mathbf{r}_1 - \mathbf{r}_i|, \dots, |\mathbf{r}_{N_c} - \mathbf{r}_i|) \frac{\partial V_{\text{eff}}(\zeta_{i,n}, |\mathbf{r}_n - \mathbf{r}_j|)}{\partial \zeta_{i,n}} \frac{\partial \zeta_{i,n}}{\partial \mathcal{E}_i} \right. \\ \left. + V_{\text{eff}}(\zeta_{i,n}, |\mathbf{r}_n - \mathbf{r}_j|) \left(\sum_{b=1}^{N_c} \frac{\partial C_{i,n}(\mathcal{E}_i, |\mathbf{r}_1 - \mathbf{r}_i|, \dots, |\mathbf{r}_{N_c} - \mathbf{r}_i|)}{\partial \zeta_{i,b}} \frac{\partial \zeta_{i,b}}{\partial \mathcal{E}_i} \right) \right] \quad (22)$$

and

$$\frac{\partial \zeta_{i,n}}{\partial \mathcal{E}_i} = \begin{cases} 0, & \mathcal{E}_i(t) \leq \mathcal{E}_{1s}^n \\ Q_n / \mathcal{E}_{1s}^n, & \mathcal{E}_{1s}^n < \mathcal{E}_i(t) < 0 \\ 0, & \mathcal{E}_i(t) \geq 0. \end{cases} \quad (23)$$

The derivatives $\frac{\partial C_{i,n}(\mathcal{E}_i, |\mathbf{r}_1 - \mathbf{r}_i|, \dots, |\mathbf{r}_{N_c} - \mathbf{r}_i|)}{\partial \zeta_{i,b}}$ and $\frac{\partial V_{\text{eff}}(\zeta_{i,n}, |\mathbf{r}_n - \mathbf{r}_j|)}{\partial \zeta_{i,n}}$ are obtained in Eqs. (B1) and (B9) of Appendix B, respectively. These derivatives are obtained in terms of the relative coordinates \mathbf{q}_k , since we propagate in the regularized coordinates system. We also find that

$$f_j = \sum_{i=N_c+1}^{N-1} \sum_{m=i+1}^N [1 - c_{i,m}(t)] \frac{Q_i Q_m (\mathbf{r}_i - \mathbf{r}_m)}{|\mathbf{r}_i - \mathbf{r}_m|^3} (\delta_{i,j} - \delta_{m,j}) \cdot \dot{\mathbf{r}}_j \\ - \sum_{\substack{i=N_c+1 \\ i \neq j}}^N \sum_{n=1}^{N_c} c_{i,j}(t) \frac{\partial C_{j,n}(\mathcal{E}_j, |\mathbf{r}_1 - \mathbf{r}_j|, \dots, |\mathbf{r}_{N_c} - \mathbf{r}_j|)}{\partial \mathbf{r}_j} V_{\text{eff}}(\zeta_{j,n}, |\mathbf{r}_n - \mathbf{r}_i|) \cdot \dot{\mathbf{r}}_j \\ + \sum_{\substack{i=N_c+1 \\ i \neq j}}^N \sum_{n=1}^{N_c} c_{i,j}(t) \left(C_{i,n}(\mathcal{E}_i, |\mathbf{r}_1 - \mathbf{r}_i|, \dots, |\mathbf{r}_{N_c} - \mathbf{r}_i|) \frac{\partial V_{\text{eff}}(\zeta_{i,n}, |\mathbf{r}_n - \mathbf{r}_j|)}{\partial \mathbf{r}_n} \right. \\ \left. + \sum_{b=1}^{N_c} V_{\text{eff}}(\zeta_{i,b}, |\mathbf{r}_b - \mathbf{r}_j|) \frac{\partial C_{i,b}(\mathcal{E}_i, |\mathbf{r}_1 - \mathbf{r}_i|, \dots, |\mathbf{r}_{N_c} - \mathbf{r}_i|)}{\partial \mathbf{r}_n} \right) \cdot \dot{\mathbf{r}}_n \\ + \sum_{n=1}^{N_c} \left(-\frac{Q_n Q_j (\mathbf{r}_n - \mathbf{r}_j)}{|\mathbf{r}_n - \mathbf{r}_j|^3} \right) \cdot \dot{\mathbf{r}}_n + \sum_{\substack{i=N_c+1 \\ i \neq j}}^N \sum_{n=1}^{N_c} c_{i,j}(t) \left(V_{\text{eff}}(\zeta_{i,n}, |\mathbf{r}_n - \mathbf{r}_j|) \frac{\partial C_{i,n}(\mathcal{E}_i, |\mathbf{r}_1 - \mathbf{r}_i|, \dots, |\mathbf{r}_{N_c} - \mathbf{r}_i|)}{\partial \mathbf{r}_i} \right) \cdot \dot{\mathbf{r}}_i \\ + \sum_{\substack{i=N_c+1 \\ i \neq j}}^N \sum_{n=1}^{N_c} \dot{c}_{i,j}(t) C_{i,n}(\mathcal{E}_i, |\mathbf{r}_1 - \mathbf{r}_i|, \dots, |\mathbf{r}_{N_c} - \mathbf{r}_i|) V_{\text{eff}}(\zeta_{i,n}, |\mathbf{r}_n - \mathbf{r}_j|) - Q_j \mathbf{r}_j \cdot \dot{\mathbf{E}}(\mathbf{r}_j, t), \quad (24)$$

where $\dot{\mathbf{r}}_n = \frac{\mathbf{p}_n}{m_n}$, $\dot{\mathbf{r}}_i = \frac{\mathbf{p}_i}{m_i}$, and $\dot{\mathbf{r}}_j = \frac{\mathbf{p}_j}{m_j}$. The derivatives of $C_{j,n}$ and V_{eff} in Eq. (24) can be found in Eqs. (B3), (B2), and (B10). These derivatives and all the terms in Eqs. (22) and (24) are obtained in terms of the relative coordinates \mathbf{q}_k since we propagate in the regularized coordinates system. For each electron we obtain an equation similar to Eq. (21). Hence, at any time during time propagation, we solve a system of $N - N_c$ equations to obtain the derivative in terms of the energy of each electron, so that it does not depend on the derivatives of the other electron energies. We solve this system of linear equations using Cramer's rule [48,49].

E. Hamilton's equations of motion

Substituting Eqs. (11) and (19) in Eq. (8), we find that the Hamiltonian in regularized coordinates is given by

$$H = \sum_{k,k'=1}^K T_{kk'} \rho_k \rho_{k'} + \frac{\langle \rho \rangle^2}{2M} + \sum_{k=1}^K [1 - c_k(t)] \frac{U_k}{q_k} + \sum_{i=1}^N \frac{Q_i^2}{2m_i} A^2(\mathbf{r}_i, t) - \sum_{i=1}^N \frac{Q_i}{m_i} \dot{\mathbf{p}}_i \cdot \mathbf{A}(\mathbf{r}_i, t) + \sum_{k=1}^K \sum_{n=1}^{N_c} c_k(t) V_{k,n}, \quad (25)$$

where $U_{k(i,j)} = Q_i Q_j$. The term $V_{k(i,j),n}$ is now given by

$$V_{k(i,j),n} = C_{j,n}(\mathcal{E}_j, |\mathbf{r}_1 - \mathbf{r}_j|, \dots, |\mathbf{r}_{N_c} - \mathbf{r}_j|) V_{\text{eff}}(\zeta_{j,n}(t), |\mathbf{r}_n - \mathbf{r}_i|) \\ + C_{i,n}(\mathcal{E}_i, |\mathbf{r}_1 - \mathbf{r}_i|, \dots, |\mathbf{r}_{N_c} - \mathbf{r}_i|) V_{\text{eff}}(\zeta_{i,n}(t), |\mathbf{r}_n - \mathbf{r}_j|) \quad (26)$$

and $\tilde{\mathbf{p}}$ and \mathbf{r} are expressed in terms of $\boldsymbol{\rho}$ and \mathbf{q} via Eqs. (19) and (18). Moreover, we set $c_k(t) = 0$ when k corresponds to the relative distance between an electron and a core. This is the case since in our model the Coulomb potential between an electron and a core is given by the full Coulomb potential. Using Eq. (25), we find that Hamilton's equations of motion are given by

$$\frac{d\mathbf{q}_k}{dt} = 2 \sum_{k'=1}^K T_{kk'} \boldsymbol{\rho}_{k'} - \sum_{i=1}^N \frac{Q_i}{m_i} \alpha_{ik} \mathbf{A}(\mathbf{r}_i, t), \\ \frac{d\langle \mathbf{q} \rangle}{dt} = \frac{1}{M} \langle \boldsymbol{\rho} \rangle - \sum_{i=1}^N \frac{Q_i}{M} \mathbf{A}(\mathbf{r}_i, t), \\ \frac{d\boldsymbol{\rho}_k}{dt} = [1 - c_k(t)] \frac{U_k \mathbf{q}_k}{q_k^3} - \sum_{k'=1}^K c_{k'}(t) h_k^{k'} + \sum_{i=1}^N \frac{Q_i}{m_i} [\tilde{\mathbf{p}}_i - Q_i \mathbf{A}(\mathbf{r}_i, t)] \cdot \frac{\partial \mathbf{A}(\mathbf{r}_i, t)}{\partial \mathbf{q}_k}, \\ \frac{d\langle \boldsymbol{\rho} \rangle}{dt} = \sum_{i=1}^N \frac{Q_i}{m_i} [\tilde{\mathbf{p}}_i - Q_i \mathbf{A}(\mathbf{r}_i, t)] \cdot \frac{\partial \mathbf{A}(\mathbf{r}_i, t)}{\partial \langle \mathbf{q} \rangle}, \quad (27)$$

where

$$\sum_{k'=1}^K c_{k'}(t) h_k^{k'} = \sum_{k'=1}^K \sum_{n=1}^{N_c} c_{k'}(t) \frac{\partial V_{k',n}}{\partial \mathbf{q}_k}. \quad (28)$$

We find $\frac{\partial V_{k',n}}{\partial \mathbf{q}_k}$ to be given by

$$\frac{\partial V_{k'(i',j'),n}}{\partial \mathbf{q}_{k(i,j)}} = \delta_{i',j} \left(\delta_{n,i} C_{j',n}(\mathcal{E}_{j'}, |\mathbf{r}_1 - \mathbf{r}_{j'}|, \dots, |\mathbf{r}_{N_c} - \mathbf{r}_{j'}|) \frac{\partial V_{\text{eff}}(\zeta_{j',n}, |\mathbf{r}_n - \mathbf{r}_{j'}|)}{\partial \mathbf{q}_k} \right. \\ \left. + \frac{\partial C_{i',n}(\mathcal{E}_{i'}, |\mathbf{r}_1 - \mathbf{r}_{i'}|, \dots, |\mathbf{r}_{N_c} - \mathbf{r}_{i'}|)}{\partial \mathbf{q}_k} V_{\text{eff}}(\zeta_{i',n}, |\mathbf{r}_n - \mathbf{r}_{j'}|) \right) + \delta_{j',j} \left(\delta_{n,i} C_{i',n}(\mathcal{E}_{i'}, |\mathbf{r}_1 - \mathbf{r}_{i'}|, \dots, |\mathbf{r}_{N_c} - \mathbf{r}_{i'}|) \right. \\ \left. \times \frac{\partial V_{\text{eff}}(\zeta_{i',n}, |\mathbf{r}_n - \mathbf{r}_{j'}|)}{\partial \mathbf{q}_k} + \frac{\partial C_{j',n}(\mathcal{E}_{j'}, |\mathbf{r}_1 - \mathbf{r}_{j'}|, \dots, |\mathbf{r}_{N_c} - \mathbf{r}_{j'}|)}{\partial \mathbf{q}_k} V_{\text{eff}}(\zeta_{j',n}, |\mathbf{r}_n - \mathbf{r}_{i'}|) \right). \quad (29)$$

Thus, for $h_k^{k'}$ we obtain

$$h_k^{k'} = \sum_{n=1}^{N_c} \frac{\partial V_{k'(i',j'),n}}{\partial \mathbf{q}_{k(i,j)}} = \delta_{i',j} \left(C_{j',i}(\mathcal{E}_{j'}, |\mathbf{r}_1 - \mathbf{r}_{j'}|, \dots, |\mathbf{r}_{N_c} - \mathbf{r}_{j'}|) \frac{\partial V_{\text{eff}}(\zeta_{j',i}, |\mathbf{r}_i - \mathbf{r}_{j'}|)}{\partial \mathbf{q}_k} \right. \\ \left. + \sum_{n=1}^{N_c} \frac{\partial C_{i',n}(\mathcal{E}_{i'}, |\mathbf{r}_1 - \mathbf{r}_{i'}|, \dots, |\mathbf{r}_{N_c} - \mathbf{r}_{i'}|)}{\partial \mathbf{q}_k} V_{\text{eff}}(\zeta_{i',n}, |\mathbf{r}_n - \mathbf{r}_{j'}|) \right) + \delta_{j',j} \left(C_{i',i}(\mathcal{E}_{i'}, |\mathbf{r}_1 - \mathbf{r}_{i'}|, \dots, |\mathbf{r}_{N_c} - \mathbf{r}_{i'}|) \right. \\ \left. \times \frac{\partial V_{\text{eff}}(\zeta_{i',i}, |\mathbf{r}_i - \mathbf{r}_{j'}|)}{\partial \mathbf{q}_k} + \sum_{n=1}^{N_c} \frac{\partial C_{j',n}(\mathcal{E}_{j'}, |\mathbf{r}_1 - \mathbf{r}_{j'}|, \dots, |\mathbf{r}_{N_c} - \mathbf{r}_{j'}|)}{\partial \mathbf{q}_k} V_{\text{eff}}(\zeta_{j',n}, |\mathbf{r}_n - \mathbf{r}_{i'}|) \right), \quad (30)$$

where the derivatives of V_{eff} and C can be found in Appendix B in Eqs. (B11) and (B4), respectively. Note that when $N_c = 1$, Hamilton's equations in Eq. (27) reduce to the corresponding equations for an atom [27].

F. Time derivative of the Hamiltonian

During propagation, besides other criteria used that we do not detail here, we check the accuracy of our propagation also by comparing the propagated Hamiltonian with the Hamiltonian obtained by substituting the propagated variables. The

time derivative of the Hamiltonian in Eq. (25) is given by

$$\frac{dH}{dt} = \sum_{k=1}^K \left(\frac{\partial H}{\partial \mathbf{q}_k} \dot{\mathbf{q}}_k + \frac{\partial H}{\partial \boldsymbol{\rho}_k} \dot{\boldsymbol{\rho}}_k \right) + \frac{\partial H}{\partial \langle \mathbf{q} \rangle} \langle \dot{\mathbf{q}} \rangle + \frac{\partial H}{\partial \langle \boldsymbol{\rho} \rangle} \langle \dot{\boldsymbol{\rho}} \rangle + \frac{\partial H}{\partial t} \\ = \sum_{k=1}^K (-\dot{\boldsymbol{\rho}}_k \dot{\mathbf{q}}_k + \dot{\mathbf{q}}_k \dot{\boldsymbol{\rho}}_k) - \langle \dot{\boldsymbol{\rho}} \rangle \langle \dot{\mathbf{q}} \rangle + \langle \dot{\mathbf{q}} \rangle \langle \dot{\boldsymbol{\rho}} \rangle + \frac{\partial H}{\partial t} \\ = \frac{\partial H}{\partial t}. \quad (31)$$

The partial derivative of the Hamiltonian with respect to time is given as

$$\begin{aligned}
 \frac{\partial H}{\partial t} &= \sum_{i=N_{c+1}}^{N-1} \sum_{j=i+1}^N g_{j,i} \dot{\mathcal{E}}_i + \sum_{k=1}^K \sum_{n=1}^{N_c} \dot{c}_k(t) V_{k,n} \\
 &\quad - \sum_{k=1}^K \dot{c}_k(t) \frac{U_k}{q_k} + \sum_{i=1}^N \frac{Q_i^2}{m_i} \mathbf{A}(\mathbf{r}_i, t) \frac{\partial \mathbf{A}(\mathbf{r}_i, t)}{\partial t} \\
 &\quad - \sum_{i=1}^N \frac{Q_i}{m_i} \tilde{\mathbf{p}}_i \cdot \frac{\partial \mathbf{A}(\mathbf{r}_i, t)}{\partial t} \\
 &= \sum_{i=N_{c+1}}^{N-1} \sum_{j=i+1}^N g_{j,i} \dot{\mathcal{E}}_i + \sum_{k=1}^K \sum_{n=1}^{N_c} \dot{c}_k(t) V_{k,n} \\
 &\quad - \sum_{k=1}^K \dot{c}_k(t) \frac{U_k}{q_k} + \sum_{i=1}^N \frac{Q_i}{m_i} \mathbf{p}_i \cdot \mathbf{E}(\mathbf{r}_i, t).
 \end{aligned} \tag{32}$$

G. Propagation technique

In our formulation, we fully account for the Coulomb singularities. Hence, an electron can approach infinitely close to the nucleus during time propagation. To ensure the accurate numerical treatment of the N -body problem in the laser field, we perform a global regularization [45] as described in Sec. II C. Here we integrate the equations of motion using a leapfrog technique [50,51] jointly with the Bulirsch-Stoer method [52,53]. This leapfrog technique allows integration of Hamilton's equation when the derivatives of the positions and the momenta depend on the quantities themselves. We previously employed this technique in our studies of nondipole effects in nonsequential double ionization of strongly driven H_2 [47] and in our studies of nonsequential triple ionization in atoms [27]. The steps involved in this technique, employed in this work, are described in detail in Ref. [27].

H. Tunneling during propagation

During time propagation, we allow for each bound electron to tunnel at the classical turning points along the axis of the electric field using the Wentzel-Kramers-Brillouin (WKB) approximation [54]. For the transmission probability we use the WKB formula for transmission through a potential barrier [54],

$$T \approx \exp\left(-2 \int_{r_a}^{r_b} \{2[V_{\text{tun}}(r, t_{\text{tun}}) - \epsilon_i]\}^{1/2} dr\right), \tag{33}$$

with $V_{\text{tun}}(r, t_{\text{tun}})$ the potential a bound electron i can tunnel through given by

$$\begin{aligned}
 V_{\text{tun}}(r, t_{\text{tun}}) &= \sum_{n=1}^{N_c} \frac{Q_n Q_i}{|\mathbf{r}_n - \mathbf{r}_i|} - Q_i \mathbf{r}_i \cdot \mathbf{E}(\mathbf{r}_i, t_{\text{tun}}) \\
 &\quad + \sum_{n=1}^{N_c} \sum_{\substack{j=N_{c+1} \\ j \neq i}}^N c_{i,j}(t_{\text{tun}}) C_{j,n}(\mathcal{E}_j, |\mathbf{r}_1 - \mathbf{r}_j|, \dots, |\mathbf{r}_{N_c} \\
 &\quad - \mathbf{r}_j|) V_{\text{eff}}(\zeta_{j,n}(t_{\text{tun}}), |\mathbf{r}_n - \mathbf{r}_i|).
 \end{aligned} \tag{34}$$

Here ϵ_i is the energy of the electron at the time of tunneling t_{tun} , and r_a and r_b are the classical turning points. We find that accounting for tunneling during time propagation is necessary in order to accurately describe phenomena related to enhanced ionization [55–59] during the fragmentation of strongly driven molecules.

I. Definition of quasifree and bound electron

In the ECBB model, the interaction between a pair of electrons where at least one is quasifree is described with the full Coulomb potential. Effective Coulomb potentials are used to describe the interaction between bound electrons. At the start of time propagation, the tunneling electron is considered quasifree and the other two electrons are bound. We decide on the fly, during time propagation, whether an electron is quasifree or bound using a simple set of criteria briefly described below [27].

A quasifree electron i transitions to bound if, following a minimum approach to the cores, the position of the electron along the field axis is influenced more by the cores than by the electric field. We assume that the electron is influenced more by the cores if its position along the electric field has at least two extrema of the same kind in a time interval less than half a period of the laser field. The minimum approach to the cores is identified by a maximum in the Coulomb potential of the quasifree electron with the cores. Also, at the end of the laser pulse, if the quasifree electron has negative compensated energy [60], this electron transitions to bound. In our studies, we use a compensated energy of an electron i that includes the effective potentials as well and is given by

$$\begin{aligned}
 \epsilon_i^{\text{comp}}(t) &= \frac{\tilde{\mathbf{p}}_i^2}{2m_i} + \sum_{n=1}^{N_c} \frac{Q_n Q_i}{|\mathbf{r}_1 - \mathbf{r}_i|} + \sum_{n=1}^{N_c} \sum_{\substack{j=N_{c+1} \\ j \neq i}}^N c_{i,j}(t) \\
 &\quad \times C_{j,n}(\mathcal{E}_j, |\mathbf{r}_1 - \mathbf{r}_j|, \dots, |\mathbf{r}_{N_c} - \mathbf{r}_j|) \\
 &\quad \times V_{\text{eff}}(\zeta_{j,n}(t), |\mathbf{r}_n - \mathbf{r}_i|).
 \end{aligned} \tag{35}$$

A bound electron i transitions to quasifree if either of the following two conditions is satisfied: (i) The compensated energy of the bound electron converges to a positive value or (ii) the magnitude of the total Coulomb potential of the electron i with the cores is smaller than a threshold value and it continuously decreases. The criteria are discussed in detail and illustrated in Ref. [27].

J. Initial conditions

1. Nuclei

In the initial state of HeH_2^+ , all three atoms are placed along the z axis. The two hydrogen atoms are at -3.09 and -1.02 a.u., respectively, and the helium atom is at 1.04 a.u., with the origin of the coordinate system set to be the center of mass of the molecule. We refer to H farther away from He as H left and the one closest to He as H middle (see Fig. 1). We compute the distance between the two hydrogen atoms and the hydrogen and helium atoms using the quantum chemistry package MOLPRO [61], employing the Hartree-Fock method with the augcc-pV5Z basis set. The Hartree-Fock method overestimates by a small amount the distance between the

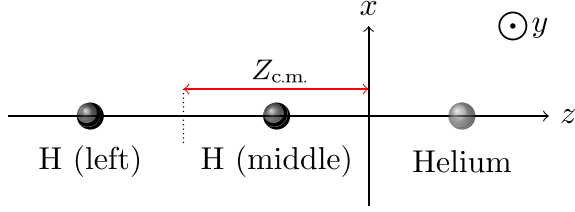


FIG. 1. Schematic illustration of the molecule under consideration, HeH_2^+ , at the time t_0 when we initialize our system. The origin of the coordinate system is set to be the center of mass of the molecule. Here $Z_{\text{c.m.}}$ is the distance between the center of mass of the molecule and the middle of the distance between H left and H middle.

hydrogen and the helium atoms [62]. However, we employ this method for consistency with the Hartree-Fock wave functions that we use in the potential energy terms involved in computing the exit point of the tunnel-ionizing electron [46]. All three nuclei are initiated at rest.

2. Tunnel-ionizing electron

The electric field is along the axis of the linear molecule, i.e., the z axis with a field strength within the below-the-barrier ionization regime. As a result, one electron (electron 1) tunnel ionizes at time t_0 through the field-lowered Coulomb potential. We employ a quantum-mechanical calculation to compute this ionization rate as described in Ref. [40]. We find t_0 , using importance sampling [63] in the time interval $[-2\tau, 2\tau]$ where the electric field is nonzero; τ is the full width at half maximum of the pulse duration in intensity. The importance sampling distribution is given by the ionization rate. We assume that electron 1 exits along the direction of the laser field; for details on the exit point, see Ref. [46]. We compute the first ionization energy of HeH_2^+ (with MOLPRO) and find it equal to 1.02 a.u. The tunnel ionizing electron exits the field-lowered Coulomb barrier with a zero momentum along the direction of the field. The transverse electron momentum is given by a Gaussian distribution. The latter arises from standard tunneling theory [64–66] and represents the Gaussian-shaped filter with an intensity-dependent width.

3. Microcanonical distribution

In the ECBB model we obtain the initial position and momentum of each bound electron i at time t_0 using a microcanonical distribution with an energy

$$\mathcal{E}_i(t_0) = \frac{\mathbf{p}_i^2}{2m_i} + W_i, \quad (36)$$

where

$$\begin{aligned} W_i = & \sum_{n=1}^{N_c} \frac{Q_n Q_i}{|\mathbf{r}_n - \mathbf{r}_i|} \\ & + \sum_{n=1}^{N_c} \sum_{\substack{j=N_c+1 \\ i \neq j}}^N c_{i,j}(t) C_{j,n}(\mathcal{E}_j, |\mathbf{r}_1 - \mathbf{r}_j|, \dots, |\mathbf{r}_{N_c} - \mathbf{r}_j|) \\ & \times V_{\text{eff}}(\zeta_{j,n}(t), |\mathbf{r}_n - \mathbf{r}_i|). \end{aligned} \quad (37)$$

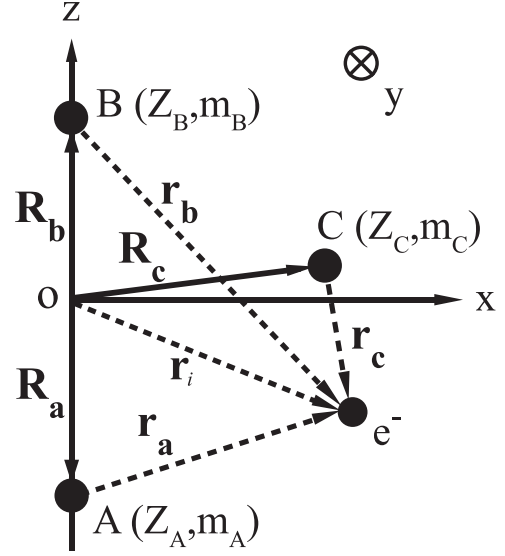


FIG. 2. Configuration of the triatomic molecule we use to set up the microcanonical distribution. The origin of the coordinate system is set to be the middle of the distance between the A and B nuclei.

We take the energy of each electron to be equal to $-I_{p,2}$, with $I_{p,2}$ the second ionization potential of the molecule under consideration. We note that the potential energy W_i of each electron i in Eqs. (36) and (37) depends not only on the coordinates of the bound electron i but also on the coordinates of all other bound electrons. This dependence is due to the function $C_{j,n}(\mathcal{E}_j, |\mathbf{r}_1 - \mathbf{r}_j|, \dots, |\mathbf{r}_{N_c} - \mathbf{r}_j|)$. Hence, the microcanonical distributions of all bound electrons are interrelated, unlike the case for atoms [27]. For a triatomic molecule, as is HeH_2^+ (the molecule considered here), indices 1–3 are reserved for the nuclei, index 4 is for the electron that tunnels in the initial state, and indices 5 and 6 are for the bound electrons. The microcanonical distribution for the two bound electrons is given by

$$\begin{aligned} f(\mathbf{r}_5, \mathbf{p}_5, \mathbf{r}_6, \mathbf{p}_6) \\ = \mathcal{N} \prod_{i=5}^6 \delta\left(\frac{p_i^2}{2} + W_i(\lambda_5, \mu_5, \phi_5, \lambda_6, \mu_6, \phi_6) - (-I_{p,2})\right), \end{aligned} \quad (38)$$

where \mathcal{N} is a normalization constant. To set up the microcanonical distribution we place the origin of our coordinate system in the middle of the distance between the nuclei A and B (see Fig. 2). As discussed at the end of this section, once we obtain the initial conditions for the position of the electrons in this coordinate system, we shift the positions with respect to the center of mass of the triatomic molecule. Moreover, λ and μ are the confocal elliptical coordinates defined using two of the nuclei as the foci of the ellipse with $\lambda \in [1, \infty)$ and $\mu \in [-1, 1]$ and are given by

$$\lambda = \frac{r_a + r_b}{R_{ab}}, \quad (39)$$

$$\mu = \frac{r_a - r_b}{R_{ab}}, \quad (40)$$

with r_a and r_b the relative position between the electron and the two nuclei labeled A and B , as shown in Fig. 2. Here R_{ab} is the distance between the two nuclei that are used to define the elliptical coordinates. The coordinate ϕ is the angle between the projection of the position vector \mathbf{r}_i of the bound electron i on the xy plane and the $+x$ axis. The z axis goes through the two nuclei that define the elliptical coordinates. Hence, the angle ϕ defines the rotation angle around the z axis (for more details see [9]). Transforming from Cartesian to elliptical coordinates, we find that the microcanonical distribution has the form

$$\begin{aligned} & \rho(\lambda_5, \mu_5, \phi_5, \lambda_6, \mu_6, \phi_6) \\ &= \mathcal{N}' \left(\frac{R_{ab}^3}{8} \right)^2 \prod_{i=5}^6 (\lambda_i^2 - \mu_i^2) \\ & \times \sqrt{2[E_i - W_i(\lambda_5, \mu_5, \phi_5, \lambda_6, \mu_6, \phi_6)]} \delta(E_i + I_{p,2}). \end{aligned} \quad (41)$$

As in our previous derivation of the microcanonical distribution for one bound electron in the presence of three nuclei [9], we find that the distribution ρ in Eq. (41) becomes infinite only when an electron is placed on top of the third nucleus, labeled C . Hence, as for our derivation in Ref. [9], to eliminate this singularity we introduce an additional transformation $t_i^\gamma = \mu_i - \mu_c$, where

$$\mu_c = \frac{R_{ac} - R_{bc}}{R_{ab}}, \quad (42)$$

with R_{ac} the distance between nuclei A and C , and similarly for the other distances. We select the value $\gamma = 3$ as the lowest one which eliminates the singularity mentioned above [9]. The final form of the microcanonical distribution is

$$\begin{aligned} & \tilde{\rho}(\lambda_5, t_5, \phi_5, \lambda_6, t_6, \phi_6) \\ &= \begin{cases} \prod_{i=5}^6 |t_i^{\gamma-1}| [|\lambda_i^2 - (t_i^\gamma + \mu_c)^2| \sqrt{P_i}] & \text{for all } P_i \geq 0 \\ 0 & \text{for any } P_i < 0, \end{cases} \end{aligned} \quad (43)$$

where

$$P_i = 2[-I_{p,2} - W_i(\lambda_5, t_5, \phi_5, \lambda_6, t_6, \phi_6)], \quad (44)$$

with

$$\begin{aligned} W_i &= \frac{Q_i Q_1}{|\mathbf{r}_1 - \mathbf{r}_i|} + \frac{Q_i Q_2}{|\mathbf{r}_2 - \mathbf{r}_i|} + \frac{Q_i Q_3}{|\mathbf{r}_3 - \mathbf{r}_i|} \\ &+ \sum_{n=1}^{N_c} \sum_{\substack{j=N_c+1 \\ j \neq i}}^N c_{i,j}(t_0) C_{j,n}(\mathcal{E}_j, |\mathbf{r}_1 - \mathbf{r}_j|, \dots, |\mathbf{r}_{N_c} - \mathbf{r}_j|) \\ &\times V_{\text{eff}}(\zeta_{j,n}(t_0), |\mathbf{r}_n - \mathbf{r}_i|), \end{aligned} \quad (45)$$

where

$$\begin{aligned} |\mathbf{r}_1 - \mathbf{r}_i| &= \frac{R_{ab}(\lambda_i + t_i^\gamma + \mu_c)}{2}, \\ |\mathbf{r}_2 - \mathbf{r}_i| &= \frac{R_{ab}(\lambda_i - t_i^\gamma - \mu_c)}{2}, \\ |\mathbf{r}_3 - \mathbf{r}_i| &= \frac{R_{ab}}{2} \left([|\lambda_i^2 + (t_i^\gamma + \mu_c)^2 - 1|] - \frac{4z_c}{R_{ab}} \lambda_i (t_i^\gamma + \mu_c) \right) \end{aligned}$$

$$\begin{aligned} &+ \frac{4(x_c^2 + z_c^2)}{R_{ab}^2} - \frac{4x_c \cos(\phi_i)}{R_{ab}} \\ &\times \sqrt{(\lambda_i^2 - 1)[1 - (t_i^\gamma + \mu_c)^2]}^{1/2}. \end{aligned} \quad (46)$$

The parameters x_c and z_c are given by

$$x_c = \pm \sqrt{R_{ac}^2 - \left(\frac{R_{ac}^2 - R_{bc}^2 + R_{ab}^2}{2R_{ab}} \right)^2}, \quad (47)$$

$$z_c = \frac{R_{ac}^2 - R_{bc}^2}{2R_{ab}}. \quad (48)$$

The new distribution $\tilde{\rho}$ goes to zero when one of the electrons is placed on top of the nucleus C , i.e., when $\lambda_i = \lambda_c = \frac{R_{ac} + R_{bc}}{R_{ab}}$, $t_i = 0$, and $\phi_i = 0, 2\pi$.

Next we generate initial conditions for the linear triatomic molecule HeH_2^+ assuming the nuclei A , B , and C correspond to the hydrogen atom on the left, to the hydrogen atom in the middle, and the helium atom, as shown in Fig. 1. We now identify the range of values of λ_i , t_i , and ϕ_i so that $P_i \geq 0$ for each bound electron i . We find that $t_i \in [t_{\min}, t_{\max}]$, and $\phi_i \in [0, 2\pi]$ for each electron, with $t_{\min} = -(1 + \mu_c)^{1/\gamma}$ and $t_{\max} = (1 - \mu_c)^{1/\gamma}$, that is, $P_i \geq 0$ is satisfied for the whole range of values of ϕ_i and t_i . In addition, for $P_i \geq 0$ to be satisfied we find that λ_i cannot be larger than λ_{\max} , i.e., $\lambda_i \in [1, \lambda_{\max}]$. The value λ_{\max} is the same for both bound electrons. For this range of values then, we find the maximum value $\tilde{\rho}_{\max}$ of the microcanonical distribution $\tilde{\rho}(\lambda_5, t_5, \phi_5, \lambda_6, t_6, \phi_6)$ given in Eq. (43). Next we generate the uniform random numbers $\lambda_i \in [1, \lambda_{\max}]$, $t_i \in [t_{\min}, t_{\max}]$, $\phi_i \in [0, 2\pi]$ for each electron, and $\chi \in [0, \tilde{\rho}_{\max}]$. If $\tilde{\rho}(\lambda_5, t_5, \phi_5, \lambda_6, t_6, \phi_6) > \chi$ then the generated values of λ_i , t_i , and ϕ_i are accepted as initial conditions; otherwise, they are rejected and the sampling process starts again. Once we find the λ_i , t_i , and ϕ_i , we obtain the position vector $\mathbf{r}_i = (r_{x,i}, r_{y,i}, r_{z,i})$ and the momentum vector $\mathbf{p}_i = (p_{x,i}, p_{y,i}, p_{z,i})$ of each electron i as

$$r_{x,i} = \frac{R_{ab} \cos(\phi_i)}{2} \sqrt{(\lambda_i^2 - 1)[1 - (t_i^\gamma + \mu_c)^2]}, \quad (49)$$

$$r_{y,i} = \frac{R_{ab} \sin(\phi_i)}{2} \sqrt{(\lambda_i^2 - 1)[1 - (t_i^\gamma + \mu_c)^2]}, \quad (50)$$

$$r_{z,i} = \frac{R_{ab} \lambda_i (t_i^\gamma + \mu_c)}{2}, \quad (51)$$

$$p_{x,i} = \sqrt{P_i} \cos(\phi_{\mathbf{p},i}) \sqrt{1 - v_{\mathbf{p},i}^2}, \quad (52)$$

$$p_{y,i} = \sqrt{P_i} \sin(\phi_{\mathbf{p},i}) \sqrt{1 - v_{\mathbf{p},i}^2}, \quad (53)$$

$$p_{z,i} = \sqrt{P_i} v_{\mathbf{p},i}, \quad (54)$$

where $\phi_{\mathbf{p},i} \in [0, 2\pi]$ and $v_{\mathbf{p},i} \in [-1, 1]$ define the momentum \mathbf{p}_i in spherical coordinates. Following the above-described formulation, we obtain the initial conditions of the electron with respect to the origin of the coordinate system. However, for our computations we need to obtain the initial conditions for the position of the electron with respect to the center of mass of the triatomic molecule. To do so, we shift the

coordinates by $\mathbf{R}_{c.m.} = (X_{c.m.}, 0, Z_{c.m.})$ with

$$X_{c.m.} = \frac{m_c x_c}{m_a + m_b + m_c}, \quad (55)$$

$$Z_{c.m.} = \frac{(m_b - m_a)R_{ab}/2 + m_c z_c}{m_a + m_b + m_c}. \quad (56)$$

For HeH_2^+ , m_a and m_b are the masses of the hydrogen atoms and m_c is the mass of the helium atom. We also note that since HeH_2^+ is a linear molecule, x_c is zero in Eqs. (45), (46), and (55). The $Z_{c.m.}$ can be seen in Fig. 1. Also, we use the parameters $I_{p,2} = -1.73$ a.u., $R_{ab} = |\mathbf{r}_1 - \mathbf{r}_2| = 2.07$ a.u., $R_{bc} = |\mathbf{r}_2 - \mathbf{r}_3| = 2.06$ a.u., $R_{ac} = |\mathbf{r}_1 - \mathbf{r}_3| = 4.12$ a.u., $Q_1 = Q_2 = 1$ a.u., and $Q_3 = 2$ a.u. The distances and the second ionization energy of HeH_2^+ were obtained using the quantum chemistry package MOLPRO [61], with the Hartree-Fock method employing the aug-cc-pV5Z basis set.

III. RESULTS

Here we employ a vector potential of the form

$$\mathbf{A}(y, t) = -\frac{E_0}{\omega} \exp \left[-2 \ln(2) \left(\frac{ct - y}{c\tau} \right)^2 \right] \sin(\omega t - ky) \hat{\mathbf{z}}, \quad (57)$$

where $k = \omega/c$ is the wave number of the laser field and τ is the full width at half maximum of the pulse duration in intensity. The direction of both the vector potential and the electric field is along the z axis. We take the propagation direction of the laser field to be along the y axis and hence the magnetic field points along the x axis. The intensity of the field is 2×10^{14} W/cm² with a pulse duration in intensity of $\tau = 40$ fs at 800 nm.

Using the ECBB model for molecules, we focus on triple ionization (TI), FTI, double ionization (DI), and FDI. Out of all events, we find that TI events account for roughly 1.2% and FTI events with $n > 2$ account for 0.3%, while DI and FDI with $n > 2$ events account for 54% and 9.5%, respectively. Hence, FDI is a major ionization process in strongly driven molecules. In triple ionization, three electrons escape and He^{2+} and two H^+ ions are formed. In frustrated triple ionization, two electrons escape and one electron finally remains bound at a Rydberg state either at He^{2+} or at one of the two H^+ ions. We also find that the formation of $\text{He}^{+*} + 2\text{H}^+$ is roughly 2.5 times more likely than the formation of $\text{He}^{2+} + \text{H}^+ + \text{H}^*$.

In double ionization, two electrons escape while one remains bound. For the vast majority of DI events, we find that the bound electron has principal quantum number $n = 1$. Also, it is three times more likely for the final fragments to be $\text{He}^+ + 2\text{H}^+$ rather than $\text{He}^{2+} + \text{H}^+ + \text{H}$, that is, in DI, it is three times more likely for the electron to remain bound at He^{2+} . In frustrated double ionization, an electron escapes, an electron remains bound at an $n = 1$ state, and another electron remains bound at a Rydberg state. In FDI, we have several possibilities for the formation of different ions depending on which ions the bound electrons are attached to. We find that it is roughly four times more likely for the deeply bound electron to remain bound at He^{2+} versus at H^+ . Here, in FTI and FDI we do not include the Rydberg $n = 2$ states, since

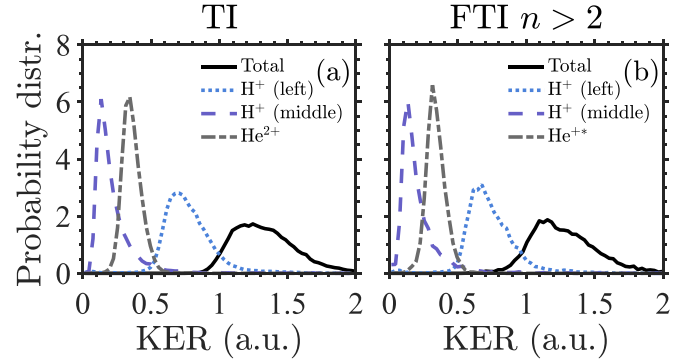


FIG. 3. Distribution of the sum of the final kinetic energies (black solid lines) of the ions produced in (a) triple ionization and (b) frustrated triple ionization. The gray dash-dotted lines depict the distribution of the final kinetic energy of the He^{2+} ion for TI and He^{+*} for FTI. The purple dashed (light blue dotted) lines depict the distribution of the final kinetic energy of the middle (left) H^+ ion for TI and FTI. All distributions are normalized to one.

an electron from the $n = 1$ state of H^+ tunnels to the $n = 2$ state of He^{2+} , resulting in a large number of $n = 2$ states. These states were also not included in our previous work on the strongly driven heteronuclear molecules HeH^+ [67] and HeH_2^+ [40].

Finally, we identify the principal quantum number n for each Rydberg electron by first calculating the classical principal quantum number

$$n_c = \frac{1}{\sqrt{2|\epsilon_i(t_f)|}}, \quad (58)$$

with $\epsilon_i(t_f)$ the energy of a bound electron at the end of the time propagation. Then we assign a quantum number n so that the following criterion is satisfied [68]:

$$\left[(n-1)(n-\frac{1}{2})n \right]^{1/3} \leq n_c \leq \left[n(n+\frac{1}{2})(n+1) \right]^{1/3}. \quad (59)$$

A. Kinetic energy release distributions

In Fig. 3 we plot the kinetic energy release (KER) of the final ion fragments for triple ionization and the most probable route to frustrated triple ionization. As expected, we find that the KERs for TI and FTI are very similar. This is consistent with the Rydberg electron in FTI remaining bound in a highly excited state. Hence, the Rydberg electron does not significantly screen the core it remains bound to. Given the similarity of the KER distributions for FTI and TI, for simplicity, we next focus on describing the features of the KER for TI. As in our previous work [40], we find that the left H^+ ion is the fastest one, followed by He^+ and the middle H^+ ion. This is consistent with both Coulomb forces exerted on the left H^+ ion being along the $-z$ axis. Similarly, both repulsive forces acting on He^+ are along the $+z$ axis. However, the mass of He is four times larger than the mass of H. This results in He^+ having a smaller acceleration and hence kinetic energy compared to the left H^+ ion. Also, the middle H^+ ion experiences repulsive forces from the left H^+ ion and from the He^+ ion in opposite directions. This small net Coulomb

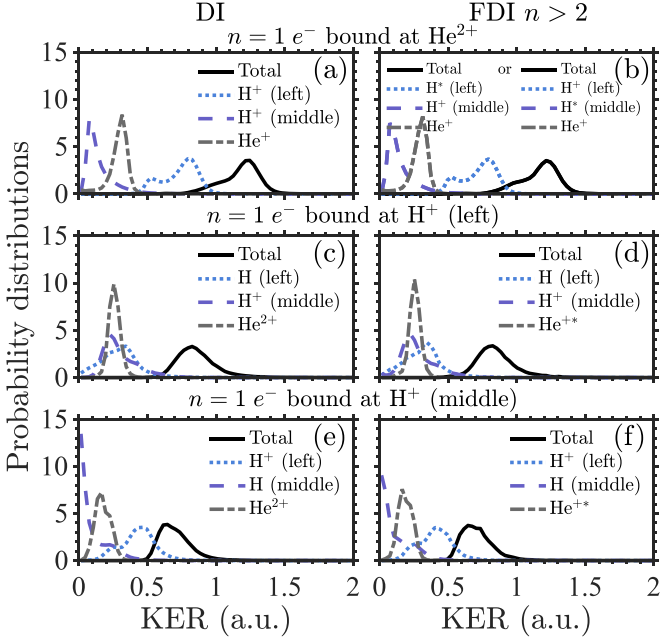


FIG. 4. Distribution of the sum of the final kinetic energies (black solid lines) of the ions produced in (a), (c), and (e) double ionization and (b), (d), and (f) frustrated double ionization with the $n = 1$ electron (a) and (b) bound at He^{2+} , (c) and (d) bound at the left H^+ ion, and (e) and (f) bound at the middle H^+ ion. The gray dash-dotted lines depict the distribution of the final kinetic energy of (a) and (b) the He^+ ion for DI and FDI and (c)–(f) He^{2+} for DI and He^{++} for FDI. The purple dashed (light blue dotted) lines depict the distribution of the final kinetic energy of (a) and (b) the middle (left) H^+ ion fragment for DI and H^* or H^+ for FDI, (c) and (d) the H^+ (H) ion for DI and FDI, and (e) and (f) the H (H^+) ion for DI and FDI. All distributions are normalized to one.

force on the middle H^+ ion results in its kinetic energy being smaller compared to the other two ions.

In Fig. 4 we plot the kinetic energy release of the final ion fragments for double and frustrated double ionization. In what follows, we focus on the most probable channels of FDI, namely, $\text{He}^+ + \text{H}^+ + \text{H}^*$ [see Fig. 4(b)], which accounts for 65% of FDI, and the channel $\text{He}^{++} + \text{H}^+ + \text{H}$ [see Figs. 4(d) and 4(f)], which accounts for 17% of FDI. We plot the KER when the bound $n = 1$ electron is attached to the He^{2+} ion [Figs. 4(a) and 4(b)], to the left H^+ ion [Figs. 4(c) and 4(d)], and to the middle H^+ ion [Figs. 4(e) and 4(f)]. As for TI and FTI, we find that the KER distributions for DI and FDI are very similar. Hence, for simplicity, we next focus on describing the features of the KER distribution for DI. When the deeply bound electron is attached to He^{2+} [Figs. 4(a) and 4(b)], we find that the left H^+ is the fastest ion, followed by He^+ and the middle H^+ ion. Indeed, the Coulomb repulsive forces on the left H^+ ion from the other two ions are both along the $-z$ axis, on He^+ both forces are along the $+z$ axis, and on the middle H^+ ion the two forces are in opposite directions. When the deeply bound electron is attached to the left H^+ ion [Figs. 4(c) and 4(d)], the electron screens the charge of the core, resulting in a smaller Coulomb repulsion between the left H fragment and He^{2+} . Hence, the kinetic energy of each of the two fragments is smaller than their

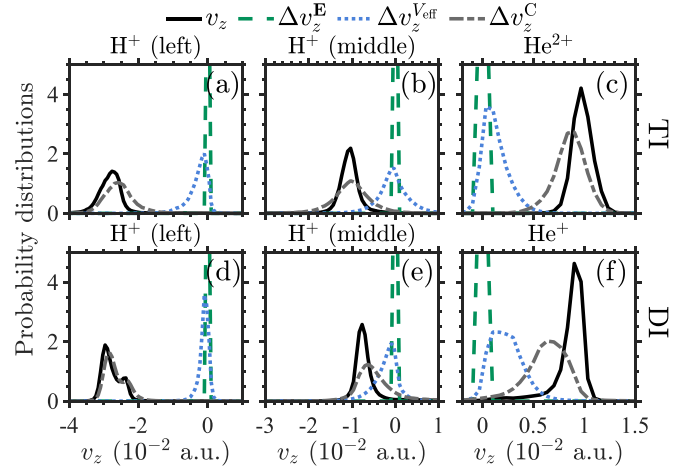


FIG. 5. Distribution of the z component of the final velocity of the ions v_z (black solid lines) and of the change of v_z in the time interval $[t_0, t_f]$ due to the forces from the electric field Δv_z^E (green dashed lines), from the effective potential $\Delta v_z^{V_{\text{eff}}}$ (light blue dotted lines), and from the Coulomb potential Δv_z^C (dark gray dash-dotted lines) for (a)–(c) TI and (d)–(f) DI with the $n = 1$ electron bound at He^{2+} .

kinetic energy when the deeply bound electron is attached to He^+ . The reduction in kinetic energy is larger for the left H fragment since both the Coulomb forces from the other two ions are now smaller. This is clearly seen by comparing the gray dash-dotted and light blue dotted lines in Fig. 4(b) with the ones in Fig. 4(a). In contrast, the total Coulomb repulsion on the middle H^+ ion is increased. Indeed, the repulsion from the left H fragment towards the z axis is decreased while the repulsion from He^{2+} towards the $-z$ axis is increased (the $n = 1$ electron is no longer attached to He^{2+}). Hence, the kinetic energy of the middle H^+ is increased [compare the purple dashed line in Fig. 4(b) with the one in Fig. 4(a)]. When the deeply bound electron is attached to the middle H^+ ion, the repulsive forces on this fragment are smaller, resulting in its smaller kinetic energy [compare the purple dashed line in Fig. 4(e) with the one in Fig. 4(c)]. Also, the kinetic energy of the left H^+ ion increases since the deeply bound electron now screens the middle H fragment [compare the light blue dotted line in Fig. 4(e) with the one in Fig. 4(c)]. Finally, the kinetic energy of He^{2+} is smaller since the deeply bound electron is attached to the H^+ ion that is closer to He^{2+} [compare the gray dash-dotted lines in Figs. 4(e) and 4(c)].

Moreover, we find that the KER distribution of the left H^+ ion has a pronounced double-peak structure for DI and FDI when the deeply bound electron is attached to He^{2+} [see the light blue dotted lines in Figs. 4(a) and 4(b)]. To identify the origin of this double peak, it suffices to focus on the DI process. In Fig. 5 we plot the final z component of the velocity of the ions along the electric field, v_z , for TI [Figs. 5(a)–5(c)] and DI [Figs. 5(d)–5(f)]. Also, we plot the contribution to this velocity from the electric field, Δv_z^E , and from the forces due to the Coulomb, Δv_z^C , and the effective, $\Delta v_z^{V_{\text{eff}}}$, potentials. For both TI and DI we find that the velocity v_z of the left H^+ ion is mostly determined by the Coulomb forces acting on this ion. For DI, the contribution of the Coulomb forces to the

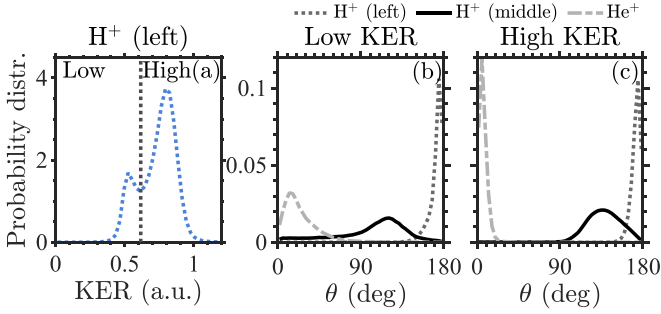


FIG. 6. (a) Distribution of the final kinetic energy of the left H^+ ion for DI when the $n = 1$ electron is bound at He^{2+} . Angular distributions of the left H^+ and middle H^+ and He^+ ions are shown for DI when the kinetic energy of the left H^+ is (b) low and (c) high.

velocity of the left H^+ ion has a clear double-peak structure [see Fig. 5(d)]. This gives rise to the double-peak structure in the kinetic energy of the left H^+ ion in Fig. 4(a). In contrast, the velocities v_z of the middle H^+ and of the He^{2+} (He^+) ion for TI (DI) are determined by the forces from both the Coulomb and the effective potential. The role of the effective potential is more pronounced for the DI process, consistent with one electron remaining bound.

Next, for DI we show how the Coulomb forces exerted on the left H^+ ion, when the deeply bound electron is attached at He^{2+} , result in a low- and a high-energy peak in the KER of the left H^+ ion [see the light blue dotted line in Fig. 4(a)]. To do so, we plot the angle of escape of each ion with respect to the z axis. The angular distributions that correspond to the low- and high-energy peaks [see Fig. 6(a)] are shown in Figs. 6(b) and 6(c), respectively. We find that the two peaks in the kinetic energy distribution of the left H^+ ion are associated with a different range of angles of escape of the middle H^+ as well as of the He^+ ions. For both peaks, the left H^+ ion escapes along the $-z$ axis [see the dark gray dotted lines in Figs. 6(b) and 6(c)]. Moreover, all ions have roughly the same charge and the middle H^+ ion is closer compared to He^+ to the left H^+ ion. Hence, it is the Coulomb repulsion between the two H^+ ions that mostly determines the final kinetic energy of the left H^+ ion. We find that for the lower-energy peak the middle H^+ ion escapes with a very wide range of angles away from the $-z$ axis, compared to a much smaller range for the high-energy peak. When the middle H^+ ion escapes with larger angles with respect to the $-z$ axis and, hence with respect to the left H^+ , the Coulomb repulsion between the two H^+ ions is smaller, resulting in a smaller kinetic energy of the left H^+ ion. In Fig. 7(b) we show that for TI the distributions of the angles of escape of the ions are very similar to the angles corresponding to the high-energy peak for DI [compare Fig. 7(b) with Fig. 6(c)]. As a result, the kinetic energy distribution of the left H^+ ion for TI is similar to the part of the distribution for DI that corresponds to the high-energy peak.

Finally, a comparison of the KER for TI, FTI, and DI obtained with the ECBB model and with the previous model in Ref. [40] reveals that the KERs have larger values for the ECBB model. This is consistent with taking into account the repulsion between the bound electrons using effective

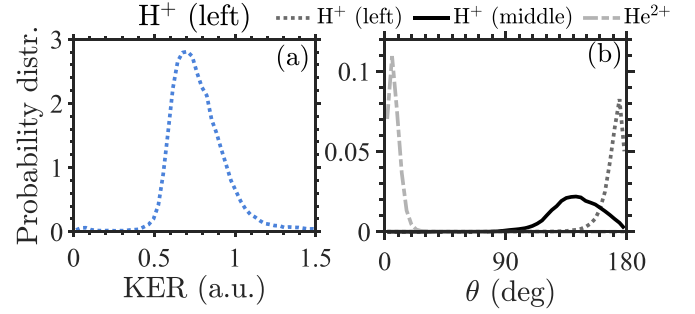


FIG. 7. (a) Distribution of the final kinetic energy of the left H^+ ion for TI. (b) Angular distributions of the left H^+ and middle H^+ and He^{2+} ions for TI.

potentials in the ECBB model. In our previous more primitive model, the repulsion between bound electrons is turned off. Due to this repulsion via the effective potentials, the electrons are less bound to the nuclei they are attached to. Hence, the electrons screen the nuclei less, leading to higher Coulomb repulsion between the nuclei and therefore to larger values of the KER. Other differences in the KER of the left and middle H^+ ions when using the ECBB model versus our previous model in Ref. [40] are due to the effective potentials in the ECBB model significantly influencing the final velocities of the middle H^+ and He^+ ions (see Fig. 5).

B. Correlation in electron escape

In Fig. 8 we plot the distribution of the difference of the ionization times between the fastest and second fastest electrons as well as the fastest and slowest electrons in TI and between the fastest and slowest electrons in FTI and DI. We find that the electron that ionizes second has a significant probability to do so with a small time difference from the fastest one, with the time difference being the smallest in TI, followed by DI and then by FTI. The distributions in all three processes extend up to ten periods (T) of the laser field. In contrast, compared to the fastest electron, the time the last electron ionizes in TI has a distribution that peaks roughly

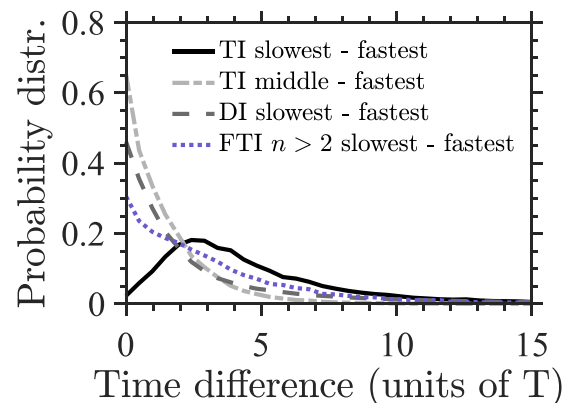


FIG. 8. Distribution of the difference of the ionization times between the fastest and second fastest electrons as well as the fastest and slowest electrons in TI and between the fastest and slowest electrons in FTI and DI.

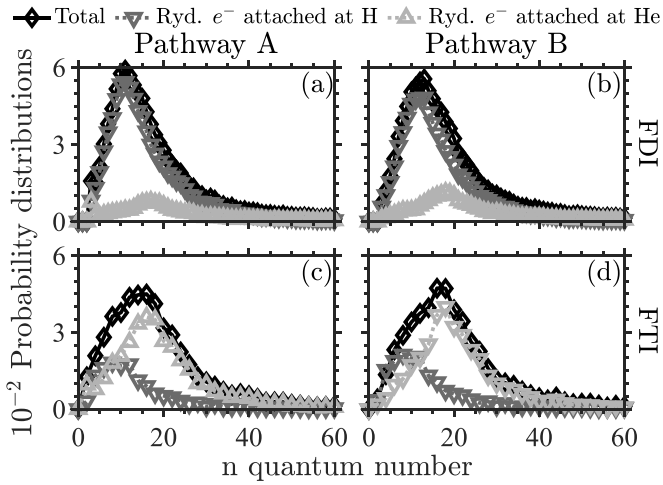


FIG. 9. Distribution of the principal n quantum number for pathways (a) A and (b) B of FDI and for pathways (c) A and (d) B of FTI (black solid lines with diamonds). The distribution of the n quantum number is also plotted separately when the Rydberg electron remains attached to He^{2+} for FTI and He^+ for FDI (light gray lines with upward pointing triangles) and when it remains attached to H^+ (dark gray lines with downward pointing triangles).

around three periods of the laser field. This suggests that the last to ionize electron escapes mainly due to enhanced ionization and not due to a recollision, i.e., the electronic correlation is weak. This is consistent with HeH_2^+ being driven by a long and intense laser pulse in the present study.

A comparison between the distributions of the difference of the ionization times for TI, FTI, and DI of HeH_2^+ obtained with the ECBB model versus its predecessor model in Ref. [40] reveals that these distributions for the ECBB model peak at smaller times and are less wide. This is consistent with the interaction between bound electrons being accounted for via effective potentials in the ECBB model. As a result, following a return of an electron to the core, energy transfer between bound electrons can take place, leading to possible ionization or excitation. This in turn leads to electrons escaping faster, which is consistent with the KER of the fragments having larger values for the ECBB model, as discussed above.

C. n quantum numbers

Next we investigate the distribution of the principal n quantum number of the two main pathways A and B of FTI and FDI (see Fig. 9). We find that FDI with $n > 2$ is a major ionization process accounting for roughly 9.5% of all events, while FTI is an order of magnitude less probable. Also, we find that pathways A (54%) and B (46%) with $n > 2$ contribute roughly the same to FTI, while for FDI pathway B contributes significantly more (70%) than pathway A. This can be understood in terms of electronic correlation. Frustrated TI, most likely, occurs when the slowest electron finally remains bound in an excited state. As for the slowest electron in TI (see the black solid line in Fig. 8), the slowest electron in FTI can gain energy both from the initially tunneling electron returning to the molecular ion and from an enhanced

ionization process. Hence, when this electron remains bound in a Rydberg state, it does so either through pathway B, related to energy gain from the returning electron, or through pathway A, related to energy gain from an enhanced ionization process [6]. Frustrated DI, most likely, occurs when the slowest of the two electrons that ionize in DI finally remains in an excited state. However, the slowest electron in DI mainly gains energy from the electron returning to the molecular ion, associated with pathway B of FDI. This is supported by the significantly faster ionization time of the second electron in DI and TI (dark gray dashed and light gray dash-dotted lines in Fig. 8) compared to the ionization times of the slowest electron in TI (black solid line in Fig. 8).

For FDI, we find that it is significantly more likely for the Rydberg electron to be attached to the H^+ ion versus the He^{2+} ion. Indeed, in Figs. 9(a) and 9(b) it can be clearly seen that the probability for the Rydberg electron to be attached to He^{2+} (area under the light gray lines with upward pointing triangles) is much smaller than the probability to be attached to one of the H^+ ions (area under the dark gray lines with downward pointing triangles). This is consistent with 65% of FDI events having the Rydberg electron attached to one of the H^+ ions, while the deeply bound electron is attached to the He^{2+} [see Fig. 4(b)]. Only 21% of FDI events have the Rydberg electron attached to He^{2+} , while the deeply bound electron is attached to one of the H^+ ions [see Figs. 4(d) and 4(f)]. The significantly higher probability for the Rydberg electron to be attached to one of the H^+ ions is consistent with the bound $n = 1$ electron staying mostly attached to the He^{2+} ion for both DI and FDI. In this case, all nuclei have a charge of roughly 1. In addition, the bound $n = 1$ electron repels the Rydberg electron from the He^+ ion, resulting in the Rydberg electron being more likely to stay bound in one of the two H^+ ions. The Rydberg electron can also remain bound at He^+ , a less likely process that we do not show in Figs. 4 and 9.

For FTI, in contrast to FDI, it is roughly 2.5 times more likely for the Rydberg electron to remain attached to He^{2+} versus the H^+ ions [compare the area under the light gray lines with upward pointing triangles and the area under the dark gray lines with downward pointing triangles in Figs. 9(c) and 9(d)]. This is consistent with an electron being significantly more likely to be attracted and remain bound at He^{2+} with charge 2 versus at H^+ with charge 1.

Also, for FDI and FTI, we find that for both pathways the distribution of the n quantum number peaks around $n = 18$ when the Rydberg electron is attached to He^{2+} compared to the significantly smaller n values when the Rydberg electron is attached to H^+ . This comes as no surprise. Indeed, we assume that the electron that tunnel ionizes last and remains bound in a Rydberg state has roughly the same energy for attachment at He^{2+} or at H^+ . Given that He^{2+} has twice the charge of H^+ , it follows that a Rydberg n state of H^+ corresponds to roughly a Rydberg $2n$ state of He^{2+} . In addition, we find that the distribution of the n number peaks at higher values for pathway A of FDI versus FTI. This is consistent with an $n = 1$ electron remaining bound in FDI, resulting in a higher screening of the cores in FDI compared to FTI and hence higher energies of the Rydberg electron for FDI.

IV. CONCLUSION

We have developed a general three-dimensional semiclassical model for the study of correlated multielectron escape during fragmentation of molecules driven by intense infrared laser pulses. This model fully accounts for the motion of all electrons and nuclei. Moreover, it is developed in the nondipole approximation, fully accounting for the magnetic field of the laser pulse. This model is a generalization of a model we previously developed for atoms. In this model, referred to as the ECBB model for molecules, the interaction of each quasifree or bound electron with the cores and each quasifree electron with a bound electron is treated exactly, fully accounting for the Coulomb singularity. To avoid artificial autoionization, the interaction of a pair of bound electrons is treated through effective Coulomb potentials. We employed the ECBB model in the context of the linear triatomic HeH_2^+ molecule. We focused our study on triple and double as well as frustrated triple and double ionization. We found that the sum of the final kinetic energies of all ion fragments is larger when described by the ECBB model versus a predecessor of the ECBB model that does not account for the interaction between

bound electrons. This suggests that the interaction between bound electrons allows for a more correlated electron-electron escape which occurs faster, leading to a Coulomb explosion of the nuclei at shorter distances. Finally, the ECBB model allows for the study of frustrated double ionization, a major ionization process. This process was not accessible with our previous models, since it has two bound electrons and the interaction between bound electrons was not accounted for. We expect that the ECBB model for strongly driven molecules will pave the way for previously inaccessible studies of multi-electron ionization processes during fragmentation of strongly driven molecules.

ACKNOWLEDGMENTS

A.E. and G.P.K. acknowledge EPSRC Grant No. EP/W005352/1. The authors acknowledge the use of the UCL Myriad High Performance Computing Facility (Myriad@UCL), the use of the UCL Kathleen High Performance Computing Facility (Kathleen@UCL), and associated support services in the completion of this work.

APPENDIX A: DERIVATION OF TERMS IN THE CHAIN RULE

We find that the terms in the chain rule in (20) are given by

$$\begin{aligned} \frac{\partial[\mathcal{E}_j(t) - H]}{\partial \mathbf{r}_j} \cdot \dot{\mathbf{r}}_j &= \frac{\partial \left(-Q_j \mathbf{r}_j \cdot \mathbf{E}(\mathbf{r}_j, t) - \sum_{i=N_c+1}^{N-1} \sum_{m=i+1}^N [1 - c_{i,m}(t)] \frac{Q_i Q_m}{|\mathbf{r}_i - \mathbf{r}_m|} \right)}{\partial \mathbf{r}_j} \cdot \dot{\mathbf{r}}_j \\ &\quad - \frac{\sum_{\substack{i=N_c+1 \\ i \neq j}}^N \sum_{n=1}^{N_c} c_{i,j}(t) C_{j,n}(\mathcal{E}_j, |\mathbf{r}_1 - \mathbf{r}_j|, \dots, |\mathbf{r}_{N_c} - \mathbf{r}_j|) V_{\text{eff}}(\zeta_{j,n}, |\mathbf{r}_n - \mathbf{r}_j|)}{\partial \mathbf{r}_j} \cdot \dot{\mathbf{r}}_j \\ &= -Q_j \mathbf{E}(\mathbf{r}_j, t) \cdot \dot{\mathbf{r}}_j + \sum_{i=N_c+1}^{N-1} \sum_{m=i+1}^N [1 - c_{i,m}(t)] \frac{Q_i Q_m (\mathbf{r}_i - \mathbf{r}_n)}{|\mathbf{r}_i - \mathbf{r}_m|^3} (\delta_{i,j} - \delta_{m,j}) \cdot \dot{\mathbf{r}}_j \\ &\quad - Q_j \mathbf{r}_j \cdot \left(\frac{\partial \mathbf{E}(\mathbf{r}_j, t)}{\partial \mathbf{r}_j} \cdot \dot{\mathbf{r}}_j \right) - \sum_{\substack{i=N_c+1 \\ i \neq j}}^N \sum_{n=1}^{N_c} c_{i,j}(t) \frac{\partial C_{j,n}(\mathcal{E}_j, |\mathbf{r}_1 - \mathbf{r}_j|, \dots, |\mathbf{r}_{N_c} - \mathbf{r}_j|)}{\partial \mathbf{r}_j} V_{\text{eff}}(\zeta_{j,n}, |\mathbf{r}_n - \mathbf{r}_j|) \cdot \dot{\mathbf{r}}_j, \end{aligned} \quad (\text{A1})$$

$$\begin{aligned} \sum_{n=1}^{N_c} \frac{\partial \mathcal{E}_j(t)}{\partial \mathbf{r}_n} \cdot \dot{\mathbf{r}}_n &= \sum_{n=1}^{N_c} \sum_{\substack{i=N_c+1 \\ i \neq j}}^N c_{i,j}(t) \sum_{b=1}^{N_c} \left(\delta_{n,b} C_{i,b} \frac{\partial V_{\text{eff}}(\zeta_{i,b}, |\mathbf{r}_b - \mathbf{r}_j|)}{\partial \mathbf{r}_n} + V_{\text{eff}}(\zeta_{i,b}, |\mathbf{r}_b - \mathbf{r}_j|) \frac{\partial C_{i,b}}{\partial \mathbf{r}_n} \right) \cdot \dot{\mathbf{r}}_n \\ &\quad + \sum_{n=1}^{N_c} \sum_{b=1}^{N_c} \left(-\delta_{n,b} \frac{Q_b Q_j (\mathbf{r}_b - \mathbf{r}_j)}{|\mathbf{r}_b - \mathbf{r}_j|^3} \right) \cdot \dot{\mathbf{r}}_n \\ &= \sum_{n=1}^{N_c} \sum_{\substack{i=N_c+1 \\ i \neq j}}^N c_{i,j}(t) \left(C_{i,n}(\mathcal{E}_i, |\mathbf{r}_1 - \mathbf{r}_i|, \dots, |\mathbf{r}_{N_c} - \mathbf{r}_i|) \frac{\partial V_{\text{eff}}(\zeta_{i,n}, |\mathbf{r}_n - \mathbf{r}_j|)}{\partial \mathbf{r}_n} + \sum_{b=1}^{N_c} V_{\text{eff}}(\zeta_{i,b}, |\mathbf{r}_b - \mathbf{r}_j|) \frac{\partial C_{i,b}}{\partial \mathbf{r}_n} \right) \cdot \dot{\mathbf{r}}_n \\ &\quad + \sum_{n=1}^{N_c} \left(-\frac{Q_n Q_j (\mathbf{r}_n - \mathbf{r}_j)}{|\mathbf{r}_n - \mathbf{r}_j|^3} \right) \cdot \dot{\mathbf{r}}_n, \end{aligned} \quad (\text{A2})$$

$$\begin{aligned} \sum_{\substack{i=N_c+1 \\ i \neq j}}^N \frac{\partial \mathcal{E}_j(t)}{\partial \mathbf{r}_i} \cdot \dot{\mathbf{r}}_i &= \sum_{\substack{i=N_c+1 \\ i \neq j}}^N \sum_{\substack{l=N_c+1 \\ l \neq j}}^N \sum_{n=1}^{N_c} c_{l,j}(t) \left(V_{\text{eff}}(\zeta_{l,n}, |\mathbf{r}_n - \mathbf{r}_j|) \delta_{i,l} \frac{\partial C_{l,n}(\mathcal{E}_l, |\mathbf{r}_1 - \mathbf{r}_l|, \dots, |\mathbf{r}_{N_c} - \mathbf{r}_l|)}{\partial \mathbf{r}_i} \right) \cdot \dot{\mathbf{r}}_i \\ &= \sum_{\substack{i=N_c+1 \\ i \neq j}}^N \sum_{n=1}^{N_c} c_{i,j}(t) \left(V_{\text{eff}}(\zeta_{i,n}, |\mathbf{r}_n - \mathbf{r}_j|) \frac{\partial C_{i,n}(\mathcal{E}_i, |\mathbf{r}_1 - \mathbf{r}_i|, \dots, |\mathbf{r}_{N_c} - \mathbf{r}_i|)}{\partial \mathbf{r}_i} \right) \cdot \dot{\mathbf{r}}_i, \end{aligned} \quad (\text{A3})$$

$$\begin{aligned} \sum_{\substack{i=N_c+1 \\ i \neq j}}^N \frac{\partial \mathcal{E}_j(t)}{\partial \mathcal{E}_i} \dot{\mathcal{E}}_i &= \sum_{\substack{i=N_c+1 \\ i \neq j}}^N \dot{\mathcal{E}}_i \sum_{\substack{l=N_c+1 \\ l \neq j}}^N \sum_{n=1}^{N_c} c_{l,j}(t) \delta_{i,l} \left(C_{l,n}(\mathcal{E}_l, |\mathbf{r}_1 - \mathbf{r}_l|, \dots, |\mathbf{r}_{N_c} - \mathbf{r}_l|) \frac{\partial V_{\text{eff}}(\zeta_{l,n}, |\mathbf{r}_n - \mathbf{r}_j|)}{\partial \mathcal{E}_i} \right. \\ &\quad \left. + V_{\text{eff}}(\zeta_{l,n}, |\mathbf{r}_n - \mathbf{r}_j|) \frac{\partial C_{l,n}(\mathcal{E}_l, |\mathbf{r}_1 - \mathbf{r}_l|, \dots, |\mathbf{r}_{N_c} - \mathbf{r}_l|)}{\partial \mathcal{E}_i} \right) \\ &= \sum_{\substack{i=N_c+1 \\ i \neq j}}^N \dot{\mathcal{E}}_i \sum_{n=1}^{N_c} c_{i,j}(t) \left(C_{i,n}(\mathcal{E}_i, |\mathbf{r}_1 - \mathbf{r}_i|, \dots, |\mathbf{r}_{N_c} - \mathbf{r}_i|) \frac{\partial V_{\text{eff}}(\zeta_{i,n}, |\mathbf{r}_n - \mathbf{r}_j|)}{\partial \mathcal{E}_i} \right. \\ &\quad \left. + V_{\text{eff}}(\zeta_{i,n}, |\mathbf{r}_n - \mathbf{r}_j|) \frac{\partial C_{i,n}(\mathcal{E}_i, |\mathbf{r}_1 - \mathbf{r}_i|, \dots, |\mathbf{r}_{N_c} - \mathbf{r}_i|)}{\partial \mathcal{E}_i} \right) \\ &= \sum_{\substack{i=N_c+1 \\ i \neq j}}^N \dot{\mathcal{E}}_i \sum_{n=1}^{N_c} c_{i,j}(t) C_{i,n}(\mathcal{E}_i, |\mathbf{r}_1 - \mathbf{r}_i|, \dots, |\mathbf{r}_{N_c} - \mathbf{r}_i|) \frac{\partial V_{\text{eff}}(\zeta_{i,n}, |\mathbf{r}_n - \mathbf{r}_j|)}{\partial \zeta_{i,n}} \frac{\partial \zeta_{i,n}}{\partial \mathcal{E}_i} \\ &\quad + \sum_{\substack{i=N_c+1 \\ i \neq j}}^N \dot{\mathcal{E}}_i \sum_{n=1}^{N_c} c_{i,j}(t) V_{\text{eff}}(\zeta_{i,n}, |\mathbf{r}_n - \mathbf{r}_j|) \sum_{b=1}^{N_c} \left(\frac{\partial C_{i,n}(\mathcal{E}_i, |\mathbf{r}_1 - \mathbf{r}_i|, \dots, |\mathbf{r}_{N_c} - \mathbf{r}_i|)}{\partial \zeta_{i,b}} \frac{\partial \zeta_{i,b}}{\partial \mathcal{E}_i} \right) \\ &= \sum_{\substack{i=N_c+1 \\ i \neq j}}^N g_{j,i} \dot{\mathcal{E}}_i, \end{aligned} \quad (\text{A4})$$

$$\begin{aligned} \frac{\partial \mathcal{E}_j(t)}{\partial t} &= \sum_{\substack{i=N_c+1 \\ i \neq j}}^N \sum_{n=1}^{N_c} \dot{c}_{i,j}(t) C_{i,n}(\mathcal{E}_i, |\mathbf{r}_1 - \mathbf{r}_i|, \dots, |\mathbf{r}_{N_c} - \mathbf{r}_i|) V_{\text{eff}}(\zeta_{i,n}, |\mathbf{r}_n - \mathbf{r}_j|) + \frac{\partial}{\partial t} \left(\frac{[\tilde{\mathbf{p}}_j - Q_j \mathbf{A}(\mathbf{r}_j, t)]^2}{2m_j} \right) - Q_j \dot{\mathbf{r}}_j \cdot \frac{\partial \mathbf{E}(\mathbf{r}_j, t)}{\partial t} \\ &= \sum_{\substack{i=N_c+1 \\ i \neq j}}^N \sum_{n=1}^{N_c} \dot{c}_{i,j}(t) C_{i,n}(\mathcal{E}_i, |\mathbf{r}_1 - \mathbf{r}_i|, \dots, |\mathbf{r}_{N_c} - \mathbf{r}_i|) V_{\text{eff}}(\zeta_{i,n}, |\mathbf{r}_n - \mathbf{r}_j|) + Q_j \dot{\mathbf{r}}_j \cdot \mathbf{E}(\mathbf{r}_j, t) - Q_j \dot{\mathbf{r}}_j \cdot \frac{\partial \mathbf{E}(\mathbf{r}_j, t)}{\partial t}. \end{aligned} \quad (\text{A5})$$

APPENDIX B: DERIVATIVES OF THE FUNCTIONS OF THE EFFECTIVE CHARGES

1. Derivatives of $C_{i,n}(\mathcal{E}_i, |\mathbf{r}_1 - \mathbf{r}_i|, \dots, |\mathbf{r}_{N_c} - \mathbf{r}_i|)$

The function $C_{i,n}(\mathcal{E}_i, |\mathbf{r}_1 - \mathbf{r}_i|, \dots, |\mathbf{r}_{N_c} - \mathbf{r}_i|)$ has the following derivative with respect to $\zeta_{i,b}$:

$$\frac{\partial C_{i,n}(\mathcal{E}_i, |\mathbf{r}_1 - \mathbf{r}_i|, \dots, |\mathbf{r}_{N_c} - \mathbf{r}_i|)}{\partial \zeta_{i,b}} = \frac{1}{(\sum_{n'=1}^{N_c} \rho_{i,n'})^2} \frac{\partial \rho_{i,b}}{\partial \zeta_{i,b}} \left(\delta_{n,b} \sum_{n'=1}^{N_c} \rho_{i,n'} - \rho_{i,n} \right). \quad (\text{B1})$$

The function $C_{i,b}(\mathcal{E}_i, |\mathbf{r}_1 - \mathbf{r}_i|, \dots, |\mathbf{r}_{N_c} - \mathbf{r}_i|)$ has the following derivative with respect to \mathbf{r}_n :

$$\frac{\partial C_{i,b}(\mathcal{E}_i, |\mathbf{r}_1 - \mathbf{r}_i|, \dots, |\mathbf{r}_{N_c} - \mathbf{r}_i|)}{\partial \mathbf{r}_n} = \frac{1}{(\sum_{n'=1}^{N_c} \rho_{i,n'})^2} \frac{\partial \rho_{i,n}}{\partial \mathbf{r}_n} \left(\delta_{n,b} \sum_{n'=1}^{N_c} \rho_{i,n'} - \rho_{i,b} \right). \quad (\text{B2})$$

The function $C_{i,n}(\mathcal{E}_i, |\mathbf{r}_1 - \mathbf{r}_i|, \dots, |\mathbf{r}_{N_c} - \mathbf{r}_i|)$ has the following derivative with respect to \mathbf{r}_i :

$$\frac{\partial C_{i,n}(\mathcal{E}_i, |\mathbf{r}_1 - \mathbf{r}_i|, \dots, |\mathbf{r}_{N_c} - \mathbf{r}_i|)}{\partial \mathbf{r}_i} = \frac{\frac{\partial \rho_{i,n}}{\partial \mathbf{r}_i} (\sum_{n'=1}^{N_c} \rho_{i,n'}) - (\sum_{n'=1}^{N_c} \frac{\partial \rho_{i,n'}}{\partial \mathbf{r}_i}) \rho_{i,n}}{(\sum_{n'=1}^{N_c} \rho_{i,n'})^2}. \quad (\text{B3})$$

The function $C_{j',n}(\mathcal{E}_{j'}, |\mathbf{r}_1 - \mathbf{r}_{j'}|, \dots, |\mathbf{r}_{N_c} - \mathbf{r}_{j'}|)$ has the following derivative with respect to \mathbf{q}_k , assuming that k can only represent electron-nucleus pairs:

$$\frac{\partial C_{j',n}(\mathcal{E}_{j'}, |\mathbf{r}_1 - \mathbf{r}_{j'}|, \dots, |\mathbf{r}_{N_c} - \mathbf{r}_{j'}|)}{\partial \mathbf{q}_{k(i,j)}} = \frac{\delta_{j',j}}{(\sum_{n'=1}^{N_c} \rho_{j',n'})^2} \frac{\partial \rho_{j',i}}{\partial \mathbf{q}_k} \left(\delta_{n,i} \sum_{n'=1}^{N_c} \rho_{j',n'} - \rho_{j',n} \right). \quad (\text{B4})$$

The function $\rho_{i,n}$ has the following derivatives with respect to \mathbf{r}_i , \mathbf{r}_n , \mathbf{q}_k , and $\zeta_{i,n}$:

$$\frac{\partial \rho_{i,n}}{\partial \mathbf{r}_i} = 2\zeta_{i,n} \frac{\mathbf{r}_n - \mathbf{r}_i}{|\mathbf{r}_n - \mathbf{r}_i|} \rho_{i,n} = 2\zeta_{i,n} \frac{\mathbf{q}_{k(n,i)}}{q_{k(n,i)}} \rho_{i,n}, \quad (\text{B5})$$

$$\frac{\partial \rho_{i,n}}{\partial \mathbf{r}_n} = -2\zeta_{i,n} \frac{\mathbf{r}_n - \mathbf{r}_i}{|\mathbf{r}_n - \mathbf{r}_i|} \rho_{i,n} = -2\zeta_{i,n} \frac{\mathbf{q}_{k(n,i)}}{q_{k(n,i)}} \rho_{i,n}, \quad (\text{B6})$$

$$\frac{\partial \rho_{i,n}}{\partial \mathbf{q}_{k(i',j')}} = \delta_{i',n} \delta_{j',i} \frac{\partial \rho_{i,n}}{\partial \mathbf{r}_n}, \quad (\text{B7})$$

$$\frac{\partial \rho_{i,n}}{\partial \zeta_{i,n}} = \left(\frac{3}{\zeta_{i,n}} - 2q_{k(n,i)} \right) \rho_{i,n}. \quad (\text{B8})$$

2. Derivatives of $V_{\text{eff}}(\zeta_{i,n}, |\mathbf{r}_n - \mathbf{r}_j|)$

The function $V_{\text{eff}}(\zeta_{i,n}, |\mathbf{r}_n - \mathbf{r}_j|)$ has the following derivative with respect to $\zeta_{i,n}$:

$$\frac{\partial V_{\text{eff}}(\zeta_{i,n}, |\mathbf{r}_n - \mathbf{r}_j|)}{\partial \zeta_{i,n}} = e^{-2\zeta_{i,n}|\mathbf{r}_n - \mathbf{r}_j|} (1 + 2\zeta_{i,n}|\mathbf{r}_n - \mathbf{r}_j|). \quad (\text{B9})$$

The function $V_{\text{eff}}(\zeta_{i,n}, |\mathbf{r}_n - \mathbf{r}_j|)$ has the following derivative with respect to \mathbf{r}_n :

$$\frac{\partial V_{\text{eff}}(\zeta_{i,n}, |\mathbf{r}_n - \mathbf{r}_j|)}{\partial \mathbf{r}_n} = \frac{-1 + [1 + 2\zeta_{i,n}|\mathbf{r}_n - \mathbf{r}_j|(1 + \zeta_{i,n}|\mathbf{r}_n - \mathbf{r}_j|)]e^{-2\zeta_{i,n}|\mathbf{r}_n - \mathbf{r}_j|}}{|\mathbf{r}_n - \mathbf{r}_j|^3} (\mathbf{r}_n - \mathbf{r}_j). \quad (\text{B10})$$

Finally, the function $V_{\text{eff}}(\zeta_{i,n}, |\mathbf{r}_n - \mathbf{r}_j|)$ has the following derivative with respect to \mathbf{q}_k :

$$\frac{\partial V_{\text{eff}}(\zeta_{j',i}, |\mathbf{r}_i - \mathbf{r}_{j'}|)}{\partial \mathbf{q}_k} = \delta_{i',j} \frac{-1 + [1 + 2\zeta_{j',i}q_k(1 + \zeta_{j',i}q_k)]e^{-2\zeta_{j',i}q_k}}{q_k^3} \mathbf{q}_k. \quad (\text{B11})$$

-
- [1] U. Eichmann, T. Nubbemeyer, H. Rottke, and W. Sandner, Acceleration of neutral atoms in strong short-pulse laser fields, *Nature (London)* **461**, 1261 (2009).
- [2] A. von Veltheim, B. Manschwetus, W. Quan, B. Borchers, G. Steinmeyer, H. Rottke, and W. Sandner, Frustrated tunnel ionization of noble gas dimers with Rydberg-electron shakeoff by electron charge oscillation, *Phys. Rev. Lett.* **110**, 023001 (2013).
- [3] V. Bendkowsky, B. Butscher, J. Nipper, J. P. Shaffer, R. Löw, and T. Pfau, Observation of ultralong-range Rydberg molecules, *Nature (London)* **458**, 1005 (2009).
- [4] W. Zhang, X. Gong, H. Li, P. Lu, F. Sun, Q. Ji, K. Lin, J. Ma, H. Li, J. Qiang, F. He, and J. Wu, Electron-nuclear correlated multiphoton-route to Rydberg fragments of molecules, *Nat. Commun.* **10**, 757 (2019).
- [5] B. Manschwetus, T. Nubbemeyer, K. Gorling, G. Steinmeyer, U. Eichmann, H. Rottke, and W. Sandner, Strong laser field fragmentation of \mathbf{H}_2 : Coulomb explosion without double ionization, *Phys. Rev. Lett.* **102**, 113002 (2009).
- [6] A. Emmanouilidou, C. Lazarou, A. Staudte, and U. Eichmann, Routes to formation of highly excited neutral atoms in the breakup of strongly driven \mathbf{H}_2 , *Phys. Rev. A* **85**, 011402(R) (2012).
- [7] T. Nubbemeyer, K. Gorling, A. Saenz, U. Eichmann, and W. Sandner, Strong-field tunneling without ionization, *Phys. Rev. Lett.* **101**, 233001 (2008).
- [8] A. Chen, H. Price, A. Staudte, and A. Emmanouilidou, Frustrated double ionization in two-electron triatomic molecules, *Phys. Rev. A* **94**, 043408 (2016).
- [9] A. Chen, C. Lazarou, H. Price, and A. Emmanouilidou, Frustrated double and single ionization in a two-electron triatomic molecule \mathbf{H}_3^+ , *J. Phys. B: At. Mol. Opt. Phys.* **49**, 235001 (2016).
- [10] A. Chen, M. F. Kling, and A. Emmanouilidou, Controlling electron-electron correlation in frustrated double ionization of triatomic molecules with orthogonally polarized two-color laser fields, *Phys. Rev. A* **96**, 033404 (2017).
- [11] G. P. Katsoulis, R. Sarkar, and A. Emmanouilidou, Enhancing frustrated double ionization with no electronic correlation in

- triatomic molecules using counter-rotating two-color circular laser fields, *Phys. Rev. A* **101**, 033403 (2020).
- [12] T. Sun, L. Zhao, Y. Liu, J. Guo, H. Lv, and H. Xu, Highly excited neutral molecules and fragment atoms of H_2 induced by strong laser fields, *Phys. Rev. A* **108**, 013120 (2023).
- [13] W. Zhang, Y. Ma, C. Lu, F. Chen, S. Pan, P. Lu, H. Ni, and J. Wu, Rydberg state excitation in molecules manipulated by bicircular two-color laser pulses, *Adv. Photonics* **5**, 016002 (2023).
- [14] W. Zhang, H. Li, X. Gong, P. Lu, Q. Song, Q. Ji, K. Lin, J. Ma, H. Li, F. Sun, J. Qiang, H. Zeng, and J. Wu, Tracking the electron recapture in dissociative frustrated double ionization of D_2 , *Phys. Rev. A* **98**, 013419 (2018).
- [15] J. McKenna, A. M. Saylor, B. Gaire, N. G. Johnson, K. D. Carnes, B. D. Esry, and I. Ben-Itzhak, Benchmark measurements of H_3^+ nonlinear dynamics in intense ultrashort laser pulses, *Phys. Rev. Lett.* **103**, 103004 (2009).
- [16] J. McKenna, A. M. Saylor, B. Gaire, N. G. Kling, B. D. Esry, K. D. Carnes, and I. Ben-Itzhak, Frustrated tunnelling ionization during strong-field fragmentation of D_3^+ , *New J. Phys.* **14**, 103029 (2012).
- [17] A. M. Saylor, J. McKenna, B. Gaire, N. G. Kling, K. D. Carnes, and I. Ben-Itzhak, Measurements of intense ultrafast laser-driven D_3^+ fragmentation dynamics, *Phys. Rev. A* **86**, 033425 (2012).
- [18] G. Pandey, S. Ghosh, and A. K. Tiwari, Dissociative ionization of the H_2 molecule under a strong elliptically polarized laser field: Carrier-envelope phase and orientation effect, *Phys. Chem. Chem. Phys.* **24**, 24582 (2022).
- [19] K. Sacha and B. Eckhardt, Nonsequential triple ionization in strong fields, *Phys. Rev. A* **64**, 053401 (2001).
- [20] P. J. Ho and J. H. Eberly, In-plane theory of nonsequential triple ionization, *Phys. Rev. Lett.* **97**, 083001 (2006).
- [21] J. H. Thiede, B. Eckhardt, D. K. Efimov, J. S. Prauzner-Bechcicki, and J. Zakrzewski, *Ab initio* study of time-dependent dynamics in strong-field triple ionization, *Phys. Rev. A* **98**, 031401(R) (2018).
- [22] D. K. Efimov, A. Maksymov, M. Ciappina, J. S. Prauzner-Bechcicki, M. Lewenstein, and J. Zakrzewski, Three-electron correlations in strong laser field ionization, *Opt. Express* **29**, 26526 (2021).
- [23] Y. Zhou, Q. Liao, and P. Lu, Complex sub-laser-cycle electron dynamics in strong-field nonsequential triple ionization, *Opt. Express* **18**, 16025 (2010).
- [24] Q. Tang, C. Huang, Y. Zhou, and P. Lu, Correlated multielectron dynamics in mid-infrared laser pulse interactions with neon atoms, *Opt. Express* **21**, 21433 (2013).
- [25] H. Jiang and F. He, Semiclassical study of nonsequential triple ionization of Ar in strong laser fields, *Phys. Rev. A* **104**, 023113 (2021).
- [26] H. Jiang, D. Efimov, F. He, and J. S. Prauzner-Bechcicki, Dalitz plots as a tool to resolve nonsequential paths in strong-field triple ionization, *Phys. Rev. A* **105**, 053119 (2022).
- [27] M. B. Peters, G. P. Katsoulis, and A. Emmanouilidou, General model and toolkit for the ionization of three or more electrons in strongly driven atoms using an effective Coulomb potential for the interaction between bound electrons, *Phys. Rev. A* **105**, 043102 (2022).
- [28] A. Emmanouilidou, M. B. Peters, and G. P. Katsoulis, Singularity in the electron-core potential as a gateway to accurate multielectron ionization spectra in strongly driven atoms, *Phys. Rev. A* **107**, L041101 (2023).
- [29] C. L. Kirschbaum and L. Wilets, Classical many-body model for atomic collisions incorporating the Heisenberg and Pauli principles, *Phys. Rev. A* **21**, 834 (1980).
- [30] R. R. Pandit, V. R. Becker, K. Barrington, J. Thurston, L. Ramunno, and E. Ackad, Comparison of the effect of soft-core potentials and Coulombic potentials on bremsstrahlung during laser matter interaction, *Phys. Plasmas* **25**, 043302 (2018).
- [31] R. R. Pandit, Y. Sentoku, V. R. Becker, K. Barrington, J. Thurston, J. Cheatham, L. Ramunno, and E. Ackad, Effect of soft-core potentials on inverse bremsstrahlung heating during laser matter interactions, *Phys. Plasmas* **24**, 073303 (2017).
- [32] P. B. Corkum, Plasma perspective on strong field multiphoton ionization, *Phys. Rev. Lett.* **71**, 1994 (1993).
- [33] R. Moshhammer, B. Feuerstein, W. Schmitt, A. Dorn, C. D. Schröter, J. Ullrich, H. Rottke, C. Trump, M. Wittmann, G. Korn, K. Hoffmann, and W. Sandner, Momentum distributions of Ne^{n+} ions created by an intense ultrashort laser pulse, *Phys. Rev. Lett.* **84**, 447 (2000).
- [34] A. Rudenko, T. Ergler, K. Zrost, B. Feuerstein, V. L. B. de Jesus, C. D. Schröter, R. Moshhammer, and J. Ullrich, From non-sequential to sequential strong-field multiple ionization: Identification of pure and mixed reaction channels, *J. Phys. B: At. Mol. Opt. Phys.* **41**, 081006 (2008).
- [35] N. Ekanayake, S. Luo, B. L. Wen, L. E. Howard, S. J. Wells, M. Videtto, C. Mancuso, T. Stanev, Z. Condon, S. LeMar, A. D. Camilo, R. Toth, W. B. Crosby, P. D. Grugan, M. F. Decamp, and B. C. Walker, Rescattering nonsequential ionization of Ne^{3+} , Ne^{4+} , Ne^{5+} , Kr^{5+} , Kr^{6+} , Kr^{7+} , and Kr^{8+} in a strong, ultraviolet, ultrashort laser pulse, *Phys. Rev. A* **86**, 043402 (2012).
- [36] O. Herrwerth, A. Rudenko, M. Kremer, V. L. B. de Jesus, B. Fischer, G. Gademann, K. Simeonidis, A. Achtelik, T. Ergler, B. Feuerstein, C. D. Schröter, R. Moshhammer, and J. Ullrich, Wavelength dependence of sub-laser-cycle few-electron dynamics in strong-field multiple ionization, *New J. Phys.* **10**, 025007 (2008).
- [37] K. Zrost, A. Rudenko, T. Ergler, B. Feuerstein, V. L. B. de Jesus, C. D. Schröter, R. Moshhammer, and J. Ullrich, Multiple ionization of Ne and Ar by intense 25 fs laser pulses: Few-electron dynamics studied with ion momentum spectroscopy, *J. Phys. B: At. Mol. Opt. Phys.* **39**, S371 (2006).
- [38] A. Rudenko, K. Zrost, B. Feuerstein, V. L. B. de Jesus, C. D. Schröter, R. Moshhammer, and J. Ullrich, Correlated multielectron dynamics in ultrafast laser pulse interactions with atoms, *Phys. Rev. Lett.* **93**, 253001 (2004).
- [39] H. Shimada, Y. Nakai, H. Oyama, K. Ando, T. Kambara, A. Hatakeyama, and Y. Yamazaki, Recoil-ion momentum spectroscopy of multiply charged argon ions produced by intense ($\sim 10^{16}$ W cm $^{-2}$) laser light, *Nucl. Instrum. Methods Phys. Res. Sect. B* **235**, 221 (2005).
- [40] M. B. Peters, V. P. Majety, and A. Emmanouilidou, Triple ionization and frustrated triple ionization in triatomic molecules driven by intense laser fields, *Phys. Rev. A* **103**, 043109 (2021).
- [41] V. J. Montemayor and G. Schiwietz, Dynamic target screening for two-active-electron classical-trajectory Monte Carlo calculations for $H^+ + He$ collisions, *Phys. Rev. A* **40**, 6223 (1989).

- [42] D. H. Kobe and K-H. Yang, Energy of a classical charged particle in an external electromagnetic field, *Eur. J. Phys.* **8**, 236 (1987).
- [43] E. Yakaboylu, M. I. Klaiber, H. Bauke, K. Z. Hatsagortsyan, and C. H. Keitel, Relativistic features and time delay of laser-induced tunnel ionization, *Phys. Rev. A* **88**, 063421 (2013).
- [44] G. P. Katsoulis, M. B. Peters, and A. Emmanouilidou, Nondipole electron momentum offset as a probe of correlated three-electron ionization in strongly driven atoms, *Phys. Rev. A* **108**, 043111 (2023).
- [45] D. C. Heggie, A global regularisation of the gravitational N -body problem, *Celest. Mech.* **10**, 217 (1974).
- [46] H. Price, C. Lazarou, and A. Emmanouilidou, Toolkit for semi-classical computations for strongly driven molecules: Frustrated ionization of H_2 driven by elliptical laser fields, *Phys. Rev. A* **90**, 053419 (2014).
- [47] G. P. Katsoulis, M. B. Peters, A. Staudte, R. Bhardwaj, and A. Emmanouilidou, Signatures of magnetic-field effects in non-sequential double ionization manifesting as backscattering for molecules versus forward scattering for atoms, *Phys. Rev. A* **103**, 033115 (2021).
- [48] G. Cramer, *Introduction à l'Analyse des Lignes Courbes Algébriques* (Cramer & Philibert, Geneva, 1750).
- [49] T. Muir, *The Theory of Determinants in the Historical Order of Development* (Dover, New York, 1960), Vol. 1.
- [50] P. Pihajoki, Explicit methods in extended phase space for inseparable Hamiltonian problems, *Celest. Mech. Dyn. Astron.* **121**, 211 (2015).
- [51] L. Liu, X. Wu, G. Huang, and F. Liu, Higher order explicit symmetric integrators for inseparable forms of coordinates and momenta, *Mon. Not. R. Astron. Soc.* **459**, 1968 (2016).
- [52] W. H. Press, S. A. Teukolsky, W. T. Vetterling, and B. P. Flannery, *Numerical Recipes: The Art of Scientific Computing*, 3rd ed. (Cambridge University Press, Cambridge, 2007).
- [53] R. Bulirsch and J. Stoer, Numerical treatment of ordinary differential equations by extrapolation methods, *Numer. Math.* **8**, 1 (1966).
- [54] E. Merzbacher, *Quantum Mechanics*, 3rd ed. (Wiley, New York, 1998).
- [55] H. Niikura, F. Légaré, R. Hasbani, A. D. Bandrauk, M. Y. Ivanov, D. M. Villeneuve, and P. B. Corkum, Sub-laser-cycle electron pulses for probing molecular dynamics, *Nature (London)* **417**, 917 (2002).
- [56] T. Zuo and A. D. Bandrauk, Charge-resonance-enhanced ionization of diatomic molecular ions by intense lasers, *Phys. Rev. A* **52**, R2511(R) (1995).
- [57] T. Seideman, M. Y. Ivanov, and P. B. Corkum, Role of electron localization in intense-field molecular ionization, *Phys. Rev. Lett.* **75**, 2819 (1995).
- [58] D. M. Villeneuve, M. Y. Ivanov, and P. B. Corkum, Enhanced ionization of diatomic molecules in strong laser fields: A classical model, *Phys. Rev. A* **54**, 736 (1996).
- [59] E. Dehghanian, A. D. Bandrauk, and G. L. Kamta, Enhanced ionization of the, *Phys. Rev. A* **81**, 061403(R) (2010).
- [60] J. G. Leopold and I. C. Percival, Ionisation of highly excited atoms by electric fields. III. Microwave ionisation and excitation, *J. Phys. B: At. Mol. Phys.* **12**, 709 (1979).
- [61] H.-J. Werner, P. J. Knowles *et al.*, MOLPRO: A package of *ab initio* programs, version 2018.1.
- [62] P. Palmieri, C. Puzzarini, V. Aquilanti, G. Capecchi, S. Cavalli, D. De Fazio, A. Aguilar, X. Giménez, and J. M. Lucas, *Ab initio* dynamics of the $He + H_2^+ \rightarrow HeH^+ + H$ reaction: A new potential energy surface and quantum mechanical cross-sections, *Mol. Phys.* **98**, 1835 (2000).
- [63] R. Y. Rubinstein and D. P. Froese, *Simulation and the Monte Carlo Method*, 3rd ed. (Wiley, Hoboken, 2016).
- [64] N. B. Delone and V. P. Krainov, Energy and angular electron spectra for the tunnel ionization of atoms by strong low-frequency radiation, *J. Opt. Soc. Am. B* **8**, 1207 (1991).
- [65] N. B. Delone and V. P. Krainov, Tunneling and barrier-suppression ionization of atoms and ions in a laser radiation field, *Phys.-Usp.* **41**, 469 (1998).
- [66] L. Fechner, N. Camus, J. Ullrich, T. Pfeifer, and R. Moshhammer, Strong-field tunneling from a coherent superposition of electronic states, *Phys. Rev. Lett.* **112**, 213001 (2014).
- [67] A. Vilà, J. Zhu, A. Scrinzi, and A. Emmanouilidou, Intertwined electron-nuclear motion in frustrated double ionization in driven heteronuclear molecules, *J. Phys. B: At. Mol. Opt. Phys.* **51**, 065602 (2018).
- [68] D. Comtois, D. Zeidler, H. Pépin, J. C. Kieffer, D. M. Villeneuve, and P. B. Corkum, Observation of Coulomb focusing in tunnelling ionization of noble gases, *J. Phys. B: At. Mol. Opt. Phys.* **38**, 1923 (2005).